UNIVERSITY OF MACEDONIA

GRADUATE PROGRAM

DEPARTMENT OF APPLIED INFORMATICS

Machine Learning-Based Identification of Paroxysmal Atrial Fibrillation from Sinus Rhythm ECG

Master Thesis

of

Myrovali Evangelia

Thessaloniki, February 2021

Machine Learning-Based Identification of Paroxysmal Atrial Fibrillation from Sinus Rhythm ECG

Evangelia Myrovali
Bachelor degree in Mathematics, Aristotle University of Thessaloniki, 2012

Master Thesis

A thesis submitted in fulfilment of the requirements for the degree of Master of Science in

APPLIED INFORMATICS

Supervising Professor
Dimitrios Hristu-Varsakelis

Approved by the three-member Examining Committee 24/02/2021

Dimitrios Hristu-Varsakelis	Ioannis Refanidis	Nikolaos Samaras
.....	.....	.....

Evangelia Myrovali

.....

Περίληψη

Η παροξυσμική κολπική μαρμαρυγή (ΠΚΜ) είναι μια αρρυθμία της καρδιάς που σχετίζεται με μειωμένη ποιότητα ζωής και αυξημένη θνησιμότητα. Η ΠΚΜ είναι μια υποκατηγορία της κολπικής μαρμαρυγής όπου εμφανίζεται σποραδικά και τερματίζεται συνήθως εντός 48 ωρών. Λόγω αυτής της φύσης της αρρυθμίας, πολλοί ασθενείς δεν έχουν επίγνωση της ΠΚΜ και συχνά δεν παρουσιάζουν κανένα σύμπτωμα. Η ΠΚΜ ανιχνεύεται όταν στο ηλεκτροκαρδιογράφημα (ΗΚΓ) υπάρχει απουσία P-κυμάτων για περισσότερο από 30 δευτερόλεπτα ή ακανόνιστος καρδιακός ρυθμός.

Σε αυτήν την εργασία στοχεύουμε στην ανίχνευση των λεπτών αλλαγών της κολπικής δραστηριότητας χρησιμοποιώντας μετρικές P-κυμάτων ικανές να υποδείξουν τους ασθενείς με ιστορικό ΠΚΜ κατά τη διάρκεια του φλεβοκομβικού ρυθμού (ΦΡ) χωρίς ορατές μεταβολές στο ΗΚΓ. Συλλέξαμε καταγραφές ΗΚΓ διάρκειας 10 λεπτών των απαγωγών X και Y κατά τη διάρκεια του ΦΡ 70 ασθενών με ιστορικό ΠΚΜ και 59 υγιών ατόμων. Για κάθε άτομο εξάγαμε σε κάθε καρδιακό κύκλο P-κύματα και υπολογίσαμε ορισμένες γνωστές μετρικές όσο και νέες που σχετίζονται με το ολοκλήρωμα και την κλίση του P-κύματος πριν και μετά απο την εφαρμογή ενός συντελεστή χρονικής κλίμακας για να ελαττώσουμε την επίδραση του καρδιακού παλμού. Λόγω του μεγάλου πλήθους των εξαγόμενων χαρακτηριστικών απο το σήμα, προσπαθήσαμε να μειώσουμε τη διάσταση του διανύσματος χρησιμοποιώντας μεθόδους επιλογής χαρακτηριστικών.

Παρατηρήσαμε στατιστικά σημαντικές διαφορές μεταξύ των εξεταζόμενων χαρακτηριστικών των ομάδων κυρίως στην απαγωγή X και δοκιμάσαμε διάφορους συνδυασμούς χαραρακτηριστικών βάσει μεθόδων επιλογής. Επιτεύχθηκε ταξινόμηση με ακρίβεια 95% η οποία είναι η μεγαλύτερη στην υπάρχουσα βιβλιογραφία χρησιμοποιώντας χαρακτηριστικά που υπολογίστηκαν με βάση το ολοκλήρωμα και την κλίση του P-κύματος της X απαγωγής. Χρησιμοποιώντας τα αποτελέσματα της εργασίας αυτής, είναι εφικτό να διευκολυνθεί η κλινική εξέταση με μη επεμβατικό τρόπο μειώνοντας το κόστος της υγιεινομικής περίλθαψης, βελτιώνοντας την ποιότητα ζωής των ασθενών και ελαχιστοποιώντας το ρίσκο ενός εγκεφαλικού επεισοδίου λόγω της έγκαιρης ανίχνευσης.

Λέξεις Κλειδιά: Παροξυσμική Κολπική μαρμαρυγή, Ηλεκτροκαρδιογράφημα, P-κύμα, Μετρικές P-κύματος, Τυχαίο δάσος

Abstract

Atrial fibrillation (AF) is a common cardiac arrhythmia which is associated with impaired quality of life and increased mortality. Paroxysmal AF (PAF) is a subtype of AF which is presented spontaneously and terminated usually within 48 hours. Because of the nature of this arrhythmia many patients are not aware of it and sometimes they don't present any symptom. AF is detected when presenting an absence of P-waves for longer than 30 s or with irregular heart rhythm.

In this work, we aim to detect subtle signs of atrial abnormality using P-waves metrics that can indicate the patients with PAF history during the sinus rhythm (SR) without presenting any visible change on ECG. We collected 10 min ECG recordings in lead X and Y during the sinus rhythm of 70 patients with PAF history and 59 healthy. For each subject we extracted beat-to-beat P-waves and we calculated some conventional metrics as well as novel ones related with P-wave's integral and slope before and after applying a time scale factor to eliminate heart rate dependence. Due to the plethora of extracted features we tried to reduce set's dimension using feature selection (FS) methods.

We observed statistical differences among the examined features of cohorts mostly in lead X and we tested several combinations based on FS methods. We achieved a maximum classification accuracy of 95% which is state of the art to the best of our knowledge using a feature set of integral and slope features of the lead-X signal. Our results were achieved using Random Forests to identify patients with PAF history from healthy ones during the SR. As a result of this work, the medical assessment in a routine clinical examination can be facilitated in a non invasive and inexpensive way as well as the quality life of patients minimising the stroke risk due to the early AF detection.

Keywords: Paroxysmal Atrial Fibrillation, ECG, P-wave, P-wave metrics, Feature selection, Random Forests

Acknowledgements

I would like to thank my supervisor Prof. Dimitrios Hristu-Varsakelis for providing professional guidance to complete this thesis after a creative, interactive, and stimulating process with innovative ideas expanding my knowledge limits. I am filled with gratitude to him, who has supported me in the challenges that I have faced as well as for his invaluable encouragement inspiring me to be the best version of myself.

I would like also to thank Prof. Vassilios Vassilikos director of 3rd Cardiology Department, Hippocration Hospital, medical school of Aristotle University of Thessaloniki for our collaboration on this interesting topic of cardiac arrhythmias. I am thankful for his guidance and expertise to advance this research study with his unique visionary interest in pioneering novel technologies and digital tools in cardiology.

Finally, I would like to thank my family for their patience, support, and kindness.

Contents

List of Figures

List of Tables

Acronyms

ECG: Electrocardiogram

AF: Atrial Fibrillation

PAF: Paroxysmal Atrial Fibrillation

SR: Sinus Rhythm

PPG: Photoplethysmogram

VCG: Vectorcardiography

HR: Heart rate

ts: Time scaling

FV: Feature vector

RF: Random Forest

OOB: Out of the bag error

FI: Feature Importance

MV: Max volume

OCI: Overlap of confidence interval

ROC: Receiver operating characteristic

FDA: Food and Drug Administration

QoL: Quality of life

ACC: Accuracy

SE: Sensitivity

SP: Specificity

AUC: Area under curve

CNN: Convolutional neural networks

BPM: Beat per minute

HF: Heart Failure

1 Introduction

In the following section, we describe the atrial fibrillation regarding demographics, diagnosis, ECG, and its types. In addition, we refer to the categories of AF detection also to the proposed methods in the literature. Moreover, we denote the aim as well as the contribution of our study to identify AF during SR.

1.1 Problem and Motivation

Cardiac diseases have been the main cause of death worldwide, based on the statistics published by the World Health Organization (WHO) from 2000 to 2016. Atrial fibrillation (AF) was discovered more than 100 years ago and is a very common cardiac disease today. About 33.5 million individuals had AF worldwide based on a multisource study in 2010. The AF widespread predominance is alarming and it is expected just in Europe that 17.9 million people could be at risk of AF by 2060. The population above the age of 35 are at higher risk of developing AF and males appear to have a higher AF incidence compared to females [11].

The gold standard for the AF diagnosis is the visual observation of the electrocardiogram (ECG). The ECG is one of the most versatile and inexpensive clinical tests over more than a century. It is the initial clinical test for diagnosing dangerous cardiac electrical disturbances related to conduction abnormalities as well as to bradyarrhythmias and tachyarrhythmias. It provides immediately available information about clinically important mechanical and metabolic problems such as myocardial ischemia/infarction, electrolyte disorders, and drug toxicity. Also, it may provide clues that allow forecasting preventable catastrophes such as sudden cardiac arrest [4].

The ECG can be recorded using noninvasive electrodes on the chest or limbs. ECG devices vary due to the number of leads that may be used and the duration of the recording. Commonly used ECG equipment in hospital settings is very sophisticated using more leads which aid in detailed heart electrical activity information as in the case in resting or stress test ECG. Therefore, this equipment is not portable, and patients are required to be at the hospital. Despite that, continuous data collection for longer intervals can be achieved utilizing implantable or wearable ECG equipment like loop monitor, patch recorders, or ambulatory devices. Thus, the user can wear them and collect ECG data anytime anywhere. Some devices can gather data continuously for more than a few days and also portable devices have the freedom of choice for the time and location [11].

The basic ECG waves are labeled alphabetically and begin with the P-wave (see Figure 1) [4]:

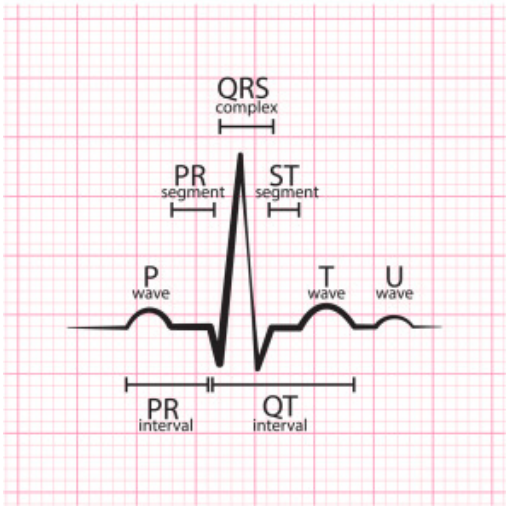

Figure 1: A typical ECG cardiac cycle.

- P wave—atrial depolarization (activation)
- QRS complex—ventricular depolarization (activation)
- ST segment, T wave, and U wave—ventricular repolarization (recovery).

The RR interval (Heart rate=60/RR in sec) is defined as the interval between two consecutive QRS complexes.

A healthy heart is described by a regular, well-organized electro-mechanical activity known as normal sinus rhythm (SR), which results in an efficient cardiac muscle contraction (heartbeat) to circulate the blood across the body. SR is the name given to the normal rhythm of the heart where electrical stimuli are initiated in the sinoatrial node causing the depolarization and subsequent contraction of the atria. The propagation then conducted through the atrioventricular node and bundle of His, bundle branches, and Purkinje fibers which rapidly depolarize the ventricles and make them strongly contract to allow an efficient pumping of blood to the lungs and the rest of the body.

Depolarization of the atria generates the P-wave, ventricular depolarization causes the impulsive QRS complex, whereas ventricular repolarization and the subsequent relaxation of the ventricular muscles are associated with the T wave. Therefore, SR is the physiologic situation in which the sinus node is generating P-waves and each P-wave is followed by a QRS complex (see Figure 2).

An irregular pulse may be an alert for AF and an ECG always is required to diagnose AF [12]. AF manifests with the absence of P-waves or with abnormal heart rhythm due to irregular contraction pattern of the atria and may be symptomatic or asymptomatic (see Figure 3). The American Heart Association (AHA), American College of Cardiology (ACC), and European Society of Cardiology (ESC)

have proposed a scheme of classification based on temporal rhythm. Thus, there are main four classes based on the frequency of AF occurrence and how long it lasts:

- *First detected*: only one diagnosed episode
- *Paroxysmal AF (PAF)*: recurrent episodes that stop on their own in less than seven days
- *Persistent AF*: recurrent episodes that last more than seven days
- *Permanent AF*: an ongoing long-term episode

First detected AF terminates itself spontaneously and followed by SR. Therefore, early detection of such episodes is almost impossible using conventional ECG monitoring solutions. ECG is examined for a certain time interval and usually when some serious symptoms have already occurred. PAF terminates by itself in less than a week and followed by SR and its detection is very difficult due to its intermittent episodic nature.

Figure 2: ECG trace of sinus rhythm.

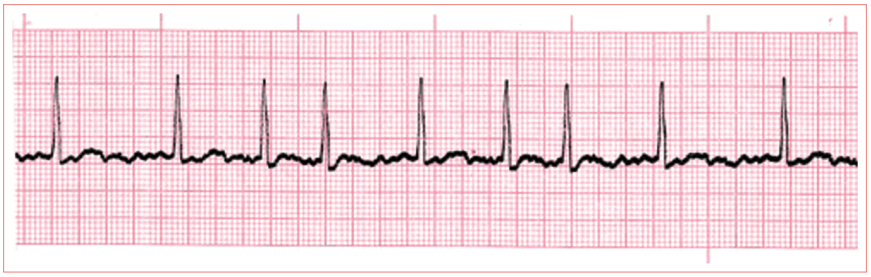

Figure 3: ECG trace of atrial fibrillation.

1.2 Literature review

Three main categories of AF detection exist in the literature. First, the AF detection in which the normal heartbeat is distinguished from AF. Therefore, the purpose is the differentiation of normal SR ECG from AF ECG segments when the AF is already present or the distinction of AF types like PAF, persistent AF (PeAF) and permanent AF. Second, the PAF prediction before it happens, and third the real-time AF detection using wearables devices [11].

1.2.1 AF real time detection using wearables ECG devices

Wearable arrhythmia detection devices based on ECG are very popular. The AliveCor KardiaBand is a Food and Drug Administration (FDA)-approved cardiac rhythm monitor that provides an automated diagnosis of either AF or SR [13]. It uses a 30-second lead I rhythm strip obtained from a single-lead electrocardiograph device paired with a smartphone. Also, it involves a machine learning algorithm to analyze electrocardiograph features and classifies the heart rhythm with sensitivity ranging from 67% to 99.6% and specificity 91% to 99% in comparison with expert cardiologist review when AF is present [14].

Moreover, AF detection can be achieved by the newest generation of smartwatches which are equipped with PPG sensors raising rhythm screening with smartphones by enabling convenient long-term screening noninvasive rhythm analysis [15]. The heart rate is measured through a smartphone's camera and flash, which are used to transilluminate capillaries in the skin for the measurement of blood flow. Changes in blood volume are synchronous with the heartbeats, such synchrony is manifested by the concordance of inter-beat intervals (RR intervals). In a PPG signal, AF is manifested as varying pulse-to-pulse intervals and pulse morphologies [16]. A smartphone application, FibriCheck, received FDA clearance for AF detection identifying pulse irregularity consistent with AF with 96% sensitivity and 97% specificity compared with cardiologist review of a 12-lead ECG.

In recent years wrist-worn wearables have gained significant recent attention for AF identification. The Apple Watch is the only commercially available wrist-based wearable with an FDA-cleared photoplethysmographic algorithm for AF detection achieving 98.3% sensitivity and 99.6% specificity in a study cohort of 301 patients with AF and 287 controls [14].

1.2.2 AF detection studies SR vs. AF

Several studies, for example [17], [18] and [19] used ECG recordings to identify SR segments versus AF or premature atrial complexes (PAC) as a prelude to AF, using deep learning methods. In particular,

Dang *et al.* [18] used heartbeat sequences P-QRS-T waves and RR-intervals which are fed into the CNN-BLSTM network model achieving an accuracy of 96.59% on test set. Further, a multi-scaled fusion of deep convolutional neural network (MS-CNN) has as inputs ECG recordings in order to capture features of different scales with an accuracy 98.13% [17]. Fan *et al.* [19] attempted to identify the premature atrial complexes (PACs) to predict the occurrence of AF by using ECG spectrograms and CNN models such as ResNet and Wide-ResNet with an accuracy of 89.2%.

1.2.3 Silent AF detection

Silent or asymptomatic AF is referred to asymptomatic episodes of AF and almost one-third of patients with AF are not aware of its presence. Consequently, AF incidence may be identified accidentally on an ECG tracing or may first present as an AF-related complication. Additionally, recent data support the assumption that silent AF is associated with morbidity and mortality rates similar to those of symptomatic AF [20]. In particular, brief, asymptomatic episodes of 5–6 min of AF are associated with increased stroke risk according to pacemaker studies [21].

The progression from paroxysmal to persistent or permanent AF might be more rapid in patients with long-term unrecognized and untreated AF. Therefore, may expose a patient to the risk of further atrial remodeling or, in patients with relatively poor ventricular rate control to tachycardia-induced cardiomyopathy resulting in significant congestive heart failure and potentially life-threatening arrhythmias [12]. The preferred methods for the silent AF detection are single 12-lead ECG recordings at outpatient visits and 24 h Holter ECG recordings; in patients with cryptogenic stroke, 24 h Holter ECG recordings are also preferred for diagnosing silent AF, while implantable ECG loop recorders are seldom used [20].

Existing AF detection algorithms and some FDA approved devices [5, 13, 16, 14] achieve very high accuracy when working with ECG signals *in which AF is actually occurring* (e.g., as high as 99.8% in [17]). However, the detection of PAF subjects when they are asymptomatic, i.e., during SR without any visible change on ECG, is more challenging.

There are few studies that attempt to find subtle variations in the cardiac cycle during SR in patients with PAF history include [22, 23] which used deep learning methods, such as CNN and data from 12-lead ECGs, to identify patients at high risk of a new AF occurrence. In addition, much of the relevant research involves some processing of P-wave signals to extract features which indicate variations in atrial activation [24] because the electrical activation of the right and left atrium is responsible for producing the P-wave in the ECG. For example, electrocardiographic indices, such as P-wave duration and morphological variability, have been shown effective in identifying subjects prone to PAF [25, 26].

Wavelet transform methods have also been proposed [27, 28], analyzing the P-wave morphologically as well as in the time-frequency domain, to extract features useful for classification or prediction.

1.3 Aims and Contribution

The silent AF detection is attracting an increasing interest due to it has been linked with stroke occurrence as well as with permanent AF. The aim of our study was the early identification of PAF during the SR on a short term ECG recording as a part of standard clinical examination. We analyzed beat-to-beat P-waves in patients with PAF history and healthy subjects from X and Y lead in order to identify the subtle differences among them. Common markers such as P-wave duration and area that related to AF as well as a new one, the P-wave slope were investigated. However, our knowledge of the P-wave area is largely based on limited studies thus, we evaluated it and formulated a novel P-wave area index.

A feature space with an abundance of extracted features was created and the use of feature selection (FS) methods was necessary for highlighting the most important features. Therefore, we formed various feature vectors that were proposed by the FS methods using Random Forests for the classification task. The area and slope of P-waves showed high classification accuracy comparable with the state of the art. Our method represents an innovative alternative to the existing literature using a feature vector of robust and descriptive features with lower computational complexity.

The present findings might help to solve the clinical challenge of identifying PAF using simple resting electrocardiographic markers. We hope that our research has several implications in therapeutic adjustments and also an impact on morbidity. In particular

- Early interventions such as pharmacological or restoration of SR can be used, thus averting PAF progression to an AF persistent type.
- Our non-invasive method can be used in clinical practice avoiding long-term electrocardiographic evaluations that increase healthcare costs.
- In a non-time-consuming approach, patients management can be facilitated enhancing their awareness by electrophysiologists.
- AF patients improve their quality of life minimizing stroke risk and invasive treatments.

1.4 Outline

The remainder of this thesis is organized as follows: the next chapter discusses important aspects of AF, including information about pathophysiology, symptoms, current clinical examination tools and common treatment approaches. Chapter 3 introduces biomedical signal processing methods on ECG and our approach to PAF identification based on P-wave ECG signal metrics. Chapter 4 contains the results from lead X and Y, feature selection methods and classification accuracy results. Chapter 5 discusses the feasibility, impact and presents a comparison with other studies. Finally, Chapter 6 summarizes our results, the implications and limitations of our proposed method as well as the future work.

2 Atrial Fibrillation

In this section, we describe the heart structure and its electrical activity using the ECG. Also, we mention the heart arrhythmias related to the atrium, AF pathophysiology and symptoms as well the screening tools to diagnose AF. In addition, we present the therapeutic approaches, pharmacologic or invasive to treat AF.

2.1 Heart structure and ECG

The heart is a muscular organ that rhythmically contracts and pumps blood to the body. It consists of four chambers, the right atrium, right ventricle, left atrium, and left ventricle, and four valves the tricuspid valve, pulmonic valve, mitral and aortic valve. Efficient pumping occurs due to the regular sequence of the different heart chambers and the presence of valves ensure unidirectional blood flow [3]. Electrical stimuli through the atria lead to atrial contraction, so the spread of stimuli through the ventricles leads to a ventricular contraction in order to pump blood to the lungs and into the general circulation [4].

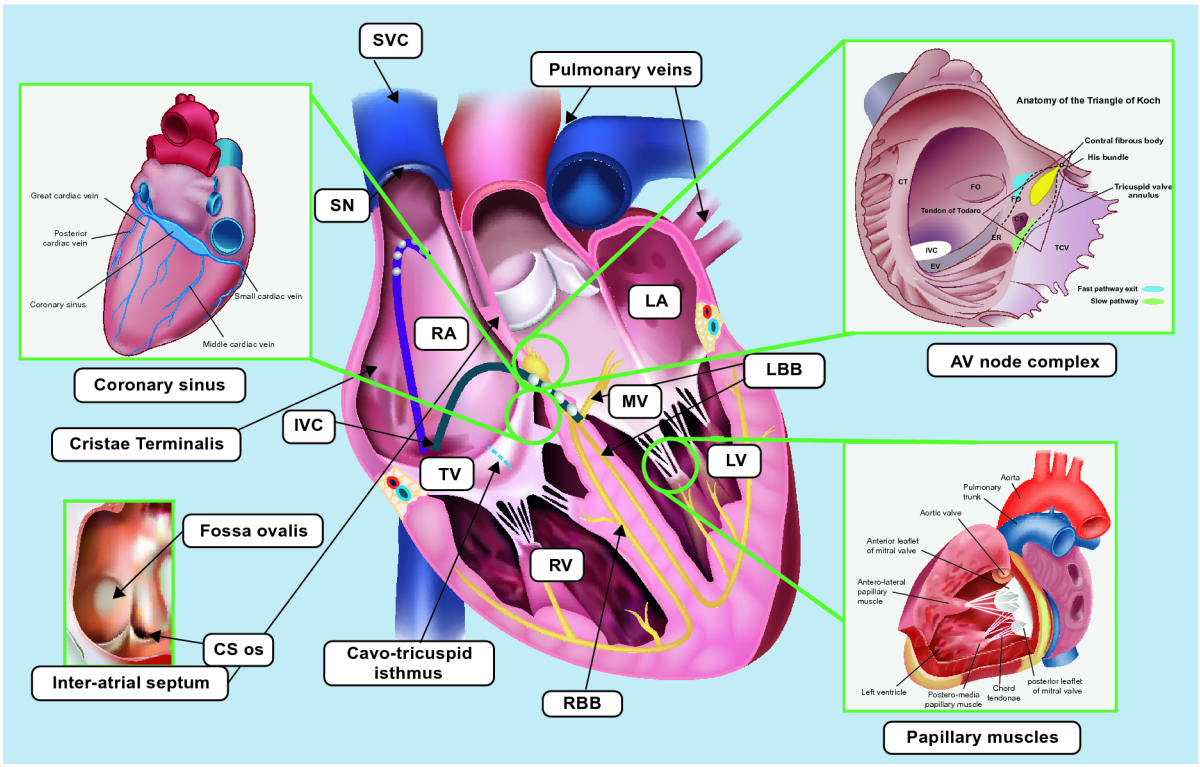

Figure 4: Basic heart anatomy; SVC: Superior vena cava, SN: Sinoatrial node, RA: Right atrium, IVC: Inferior vena cava, TV: Tricuspid valve, RV: Right ventricle, RBB: Right bundle branch, LV: Left ventricle, LBB: Left bundle branch, MV: Mitral valve, LA: Left atrium [1].

The signal for heartbeat initiation starts in the sinus or sinoatrial (SA) node. The SA node is a

small collection of specialized cells capable of automatically generating an electrical stimulus (spark-like signal) and functions as the normal pacemaker of the heart. From the sinus node, this stimulus spreads first through the right atrium and then into the left atrium. Electrical stimulation of the right and left atria signals the atria to contract and pump blood simultaneously through the tricuspid and mitral valves into the right and left ventricles. Next, it spreads through the atrioventricular (AV) node and the bundle of His, which compose the AV junction connecting the atria and ventricles. The stimulus then passes into the left and right ventricles by way of the left and right bundle branches, which are continuations of the bundle of His. Finally, the cardiac stimulus spreads to the ventricular muscle cells through the Purkinje fibers (see Figure 4) [4].

Normal "resting" myocardial cells (atrial and ventricular cells recorded between heartbeats) are polarized; that is, they carry electrical charges on their surface. When a heart muscle cell is stimulated, it depolarizes. As a result the outside of the cell, in the area where the stimulation has occurred, becomes negative and the inside of the cell becomes positive. This produces a difference in electrical voltage on the outside surface of the cell between the stimulated depolarized area and the unstimulated polarized area. The depolarizing electrical current is recorded by the ECG as a P-wave (when the atria are stimulated and depolarize) and as a QRS complex (when the ventricles are stimulated and depolarize). After a time the fully stimulated and the depolarized cell begins to return to the resting state. This is known as repolarization. A small area on the outside of the cell becomes positive again, and the repolarization spreads along the length of the cell until the entire cell is once again fully repolarized. Ventricular repolarization is recorded by the ECG as the ST segment, T wave, and U wave (see Figure 5) [4].

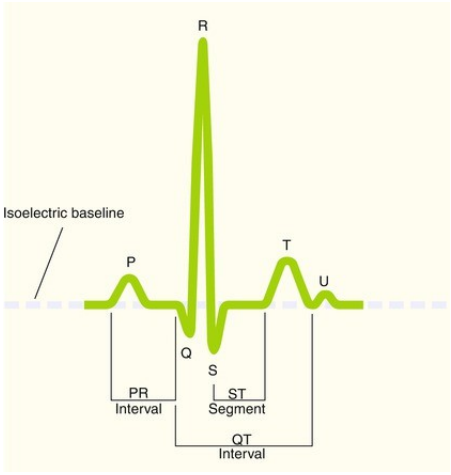

Figure 5: A typical ECG cardiac cycle and wave deflections [2].

The body acts as a conductor of electricity. Therefore, recording electrodes placed some distance

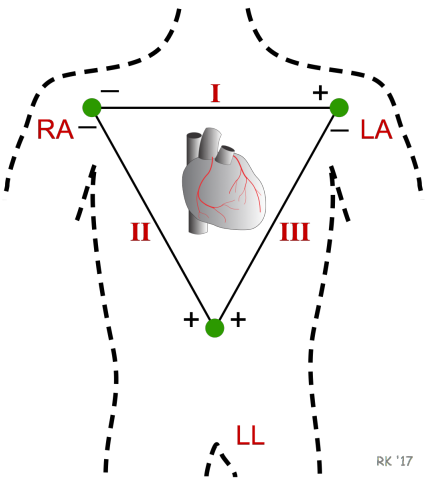

Figure 6: Einthoven triangle; Spatial orientation of the three standard limb leads I, II, and III [3].

from the heart, such as on the arms, legs, or chest wall, are able to detect the voltages of the cardiac currents conducted to these locations. The usual way of recording these voltages from the heart is with the 12 standard ECG leads. The leads actually show the differences in voltage (potential) among electrodes placed on the surface of the body. Leads I, II, and III can be represented schematically in terms of a triangle, called Einthoven's triangle after the Dutch physiologist (1860-1927) who invented the electrocardiograph (see Figure 6). Bipolar leads are related by the following simple equation in which adding the voltage in lead I to that in lead III is produced the voltage in lead II:

$$V(LeadI) + V(LeadIII) = V(LeadII)$$

The six limb leads—I, II, III, aVR, aVL, and aVF— record voltage differences by means of electrodes placed on the extremities. In addition, they can be further divided into two subgroups based on their historical development: three standard bipolar limb leads (I, II, and III) and three augmented unipolar limb leads (aVR, aVL, and aVF). The six chest leads—V1, V2, V3, V4, V5, and V6— record voltage differences by means of electrodes placed at various positions on the chest wall. The 12 ECG leads can also be viewed as 12 "channels." The 12 ECG channels (leads) are all focused on the P-QRS-T cycle, with each lead viewing it from a different angle (see Figure 7) [4].

The limb leads consist of standard bipolar (I, II, and III) and augmented (aVR, aVL, and aVF) leads. The bipolar leads record the differences in electrical voltage between two extremities (see Figure 6 and Figure 8) [4, 3].

- Lead I records the difference in voltage between the left arm (LA) and right arm (RA) electrodes:

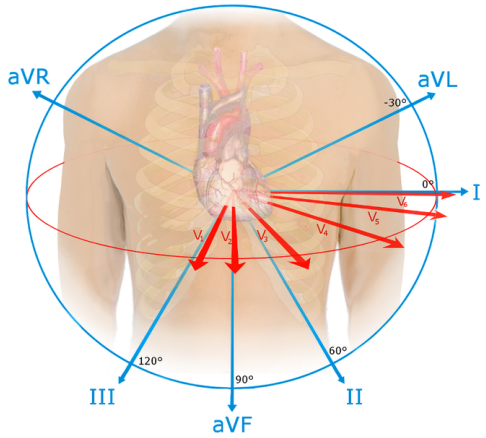

Figure 7: Spatial orientation of ECG leads; the limb leads sees the heart from vertical plane and the chest leads in horizontal plane.

Lead I=LA-RA

This axis goes from shoulder to shoulder, with the negative electrode placed on the right shoulder and the positive electrode placed on the left shoulder. This results in a 0-degree angle of orientation [29].

- Lead II records the difference between the left leg (LL) and right arm (RA) electrodes:

  Lead II=LL-RA

  This axis goes from the right arm to the left leg, with the negative electrode on the shoulder and the positive one on the leg. This results in a +60 degree angle of orientation [29].

- Lead III records the difference between the left leg (LL) and left arm (LA) electrodes:

  Lead III =LL-LA

  This axis goes from the left shoulder (negative electrode) to the right or left leg (positive electrode). This results in a +120 degree angle of orientation [29].

If the three limbs of Einthoven's triangle (assumed to be equilateral) are broken apart, collapsed, and superimposed over the heart, then the positive electrode for lead I is said to be at zero degrees relative to the heart (along the horizontal axis between LL and RA, see Figure 8). Similarly, the positive electrode for lead II (RA-LL axis) will be +60° relative to the heart, and the positive electrode for lead III (LA-LL axis) will be +120° relative to the heart as shown to the right. This new construction of the electrical axis is called the axial reference system. With this system, a wave of depolarization traveling at +60° produces the greatest positive deflection in lead II. A wave of depolarization oriented +90° relative to

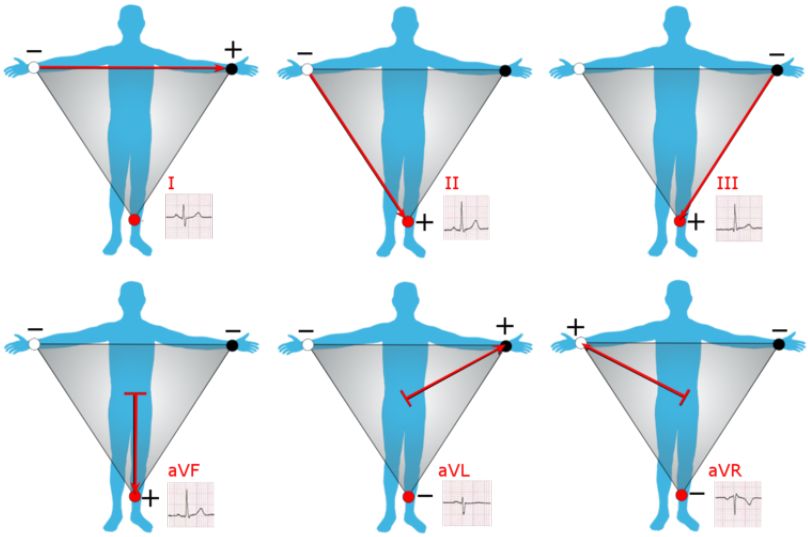

Figure 8: The limb leads I, II, III and augmented limb leads aVF, aVL, aVR.

the heart produces equally positive deflections in both lead II and III [3].

Because the heart is a three-dimensional structure the 12-leads provide a three-dimensional view of the electrical activity of the heart. Specifically, the six limb leads (I, II, III, aVR, aVL, and aVF) record electrical voltages transmitted onto the frontal plane of the body. The six chest leads (V1 to V6) record heart voltages transmitted onto the horizontal plane of the body. Together these 12 leads provide a three-dimensional picture of atrial and ventricular depolarization and repolarization (see Figure 7) [3].

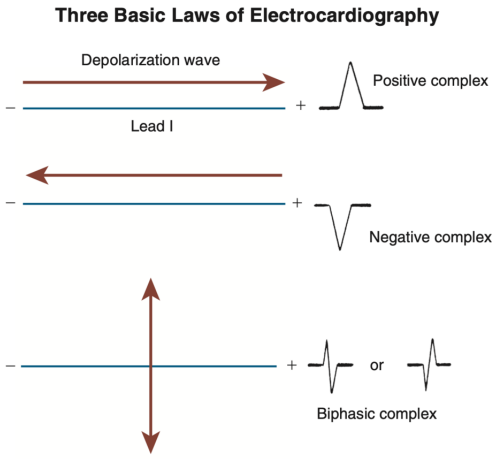

Figure 9: The three basic ECG laws based on the volume conductor model [4].

In the resting, polarized state, no potential difference is measured between the positive and negative electrodes i.e., isoelectric - flat line (see Figure 5) [3]. A positive (upward) deflection appears in any lead

if the wave of depolarization traveling toward a positive electrode. A negative (downward) deflection appears in any lead if the wave of depolarization traveling away from a positive electrode. If the mean depolarization path is directed at right angles (perpendicular) to any lead, a small biphasic deflection (consisting of positive and negative deflections of equal size) is usually seen. If the atrial stimulation path spreads at right angles to any lead, a biphasic P wave is seen in that lead (see Figure 9) [4].

The shape of the P-wave in each of the 12 standard ECG leads should be consistent with a "typical P vector" of +50° to +80°. This means that the P-wave should be:

- always positive in lead I, lead II, and aVF
- always negative in lead aVR
- any of biphasic (-/+), positive or negative in lead aVL
- positive in all chest leads, except for V1 which may be biphasic (+/-)

2.2 Types of Atrial Arrhythmias

Arrhythmias are classified not only by where they originate in the atria or the ventricles but also by the speed of heart rate they cause. Normal sinus rhythm in a resting subject is usually defined as SR with normal (1:1) AV conduction and a normal PR interval at a heart rate between 60 and 100 beats/min. SR with a heart rate of more than 100 beats/min is termed sinus tachycardia and SR with a heart rate below 60 beats/min is called sinus bradycardia. Tachycardias originating in the *atria* include atrial fibrillation, atrial flutter, supraventricular tachycardia, and Wolff-Parkinson-White syndrome. Moreover,

- Atrial fibrillation is a rapid heart rate caused by chaotic electrical impulses in the atria. These signals result in rapid, uncoordinated, weak contractions of the atria. The chaotic electrical signals bombard the AV node, usually resulting in an irregular, rapid rhythm of the ventricles.
- Atrial flutter is similar to atrial fibrillation. The heartbeats in atrial flutter are more-organized and more-rhythmic electrical impulses than in atrial fibrillation. Atrial flutter may also lead to serious complications such as stroke.
- Supraventricular tachycardia is a broad term that includes many forms of arrhythmia originating above the ventricles (supraventricular) in the atria or AV node. These types of arrhythmia seem to cause sudden episodes of palpitations that begin and end abruptly.

- In Wolff-Parkinson-White syndrome, a type of supraventricular tachycardia, there is an extra electrical pathway between the atria and the ventricles, which is present at birth. However, you may not experience symptoms until you're an adult. This pathway may allow electrical signals to pass between the atria and the ventricles without passing through the AV node, leading to short circuits and rapid heartbeats.

2.3 AF Pathophysiology and Demographics

The underlying mechanisms for the initiation and maintenance of AF have been elucidated in the last decades. AF is described by high-frequency excitation of the atrium that results in both dyssynchronous atrial contraction and irregularity of ventricular excitation [30]. Alterations in atrial refractoriness, changes in cellular calcium homeostasis, autonomic activation and delayed or early after-depolarizations can contribute to the triggered activity or ectopic focal discharges that initiate AF. Furthermore, structural abnormalities such as atrial dilatation/stretch, fibrosis, fatty infiltration, and inflammation can contribute to local conduction disturbances and conduction block that are known to facilitate re-entry and AF sustenance [31].

The AF genesis is that rapid triggering initiates propagating reentrant waves in a vulnerable atrial substrate. The pulmonary veins impact AF initiation because they have unique electric properties and a complex fiber architecture that promotes reentry and ectopic activity. Focal ectopic firing arising from myocyte sleeves within the pulmonary veins in patients with PAF. Therefore, ablation of these ectopic foci reduced the AF burden. Further, the propagating wavefront must complete one circus movement in a time period long enough for atrial tissue within that circuit to recover excitability mentioned as effective refractory period (ERP). Structural, architectural, and electrophysiological atrial abnormalities promote the perpetuation of AF by stabilizing reentry. Thus, slow conduction velocity and a short ERP promote reentry as well as molecular and histological changes impair normal anisotropic conduction (fibrosis and reduced cell coupling) and may shorten atrial ERP [30].

AF is the most common cardiac arrhythmia affecting 2–4% of the general population and a 2.3-fold rise is expected in the coming decades [5]. AF is a major health problem associated with significant morbidity and mortality as well as increased healthcare costs. There are many risk factors for AF development such as hypertension, diabetes mellitus, heart failure, coronary artery disease, chronic kidney disease, obesity, and obstructive sleep apnoea. In addition, potential contributors to the development and progression of AF are excessive alcohol consumption, smoking, sedentary lifestyles, and extreme exercise [5].

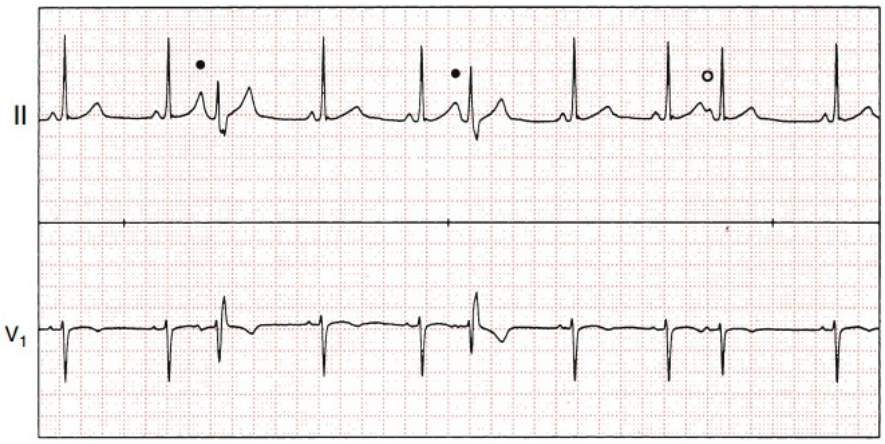

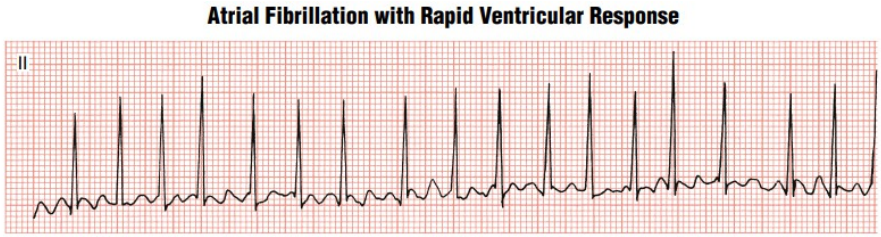

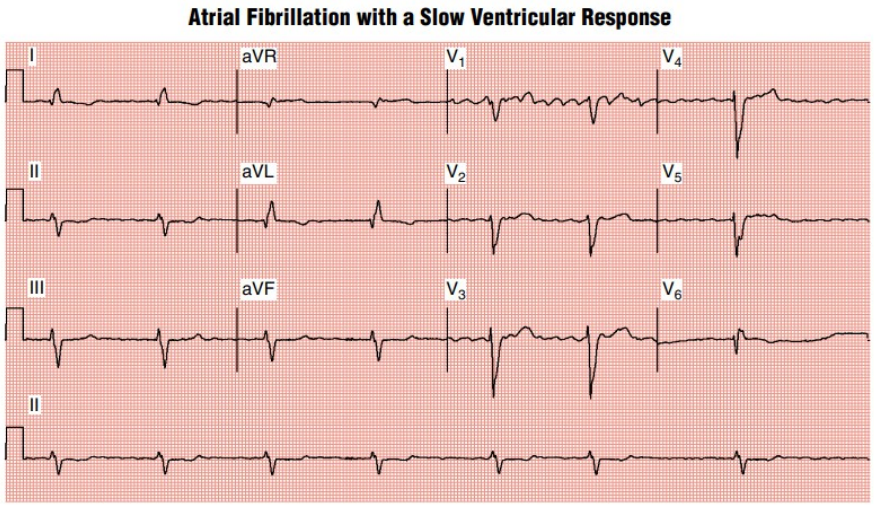

Figure 10: Top figure shows ECG in SR with three atrial premature beats in lead II, V1; the bottom figures present AF with rapid ventricular response in lead II, and AF with slow ventricular responses in 12-leads [4].

The risk factors that are associated with the incidence of AF are demographic, health behaviors, cardiovascular conditions, disorders of heart rhythm, and genetic factors. Women are less prone to AF compared with men and in non-white (i.e. Asian, African American, and Hispanic) ethnic cohorts compared with white populations. Approximately 1 in 4 individuals are going to develop AF in their life whereas 1 in 3 individuals of European ancestry at an index age of 55 years. The lifetime risk of AF is increased from 23.4% among individuals with an optimal clinical risk factor profile to 33.4% and 38.4% in those with borderline and elevated clinical risk factors [32].

2.4 Symptoms

The most frequent AF-related symptoms that patients usually experience are palpitations, dyspnoea, and fatigue whereas there are a proportion of individuals 50-87% who are initially asymptomatic or silent. Also, they may complain of chest tightness/pain, dizziness, syncope, and disordered sleep. Further, the patients that have AF symptoms are distinguished into two main categories, hemodynamically stable and unstable. Symptomatic individuals are hemodynamically unstable and they experienced syncope, hypotension, acute heart failure, myocardial ischemia, and cardiogenic shock [5]. In addition, patients with PAF mention more symptoms (80%) than those with permanent AF (51%). However, AF frequently is associated with comorbidity of stroke, systemic embolism or left ventricular (LV) dysfunction, and heart failure (HF). Of all patients with an ischaemic stroke, 20% would develop AF and prevalent HF was reported in 33%, 44%, and 56% of patients with paroxysmal, persistent, and permanent AF, respectively [32].

AF is independently related with a twofold increased risk of all-cause mortality in women and a 1.5-fold increase in men with an overall 3.5-fold mortality risk increase. The most common causes of death among AF patients were HF (14.5%), malignancy (23.1%), and infection/sepsis (17.3%), whereas stroke-related mortality was only 6.5%. Moreover, approximately 30% of AF patients have at least one, and 10% have more than two hospital admissions annually. More than 60% of AF patients have significantly impaired quality of life (QoL), exercise tolerance, but only 17% have disabling symptoms. Additionally, QoL is significantly lower in women, young individuals, and those with comorbidities [5].

2.5 Diagnosis of AF and Screening tools

The diagnosis of AF requires rhythm documentation with an electrocardiogram (ECG) tracing showing AF.

Electrocardiographic characteristics of AF include (see Figure 10 bottom):

- Irregularly irregular R-R intervals
- Absence of distinct repeating P-waves
- Irregular atrial activations

Electrical activity during AF was first recorded by means of a surface electrocardiogram and published by William Einthoven in 1906. The surface electrocardiogram is, however, a limited diagnostic tool as it only shows whether or not AF is present at the moment of recording, without providing any information on the underlying mechanism. To overcome this limitation, electrocardiographic body surface mapping techniques using multiple electrodes (up to 252) to detect electrical activity during AF have been developed. Not only surface electrocardiograms, but also endocardial or epicardial (non)-contact electrograms have been used to study the physiology of AF. However, despite the enormous technological progress in recent years and the diversity of mapping technologies currently available, the pathophysiology of AF is still not completely understood [33].

AF-screening can reveal heart abnormalities preventing arrhythmia progression. However, only 1.5% of single-time point ECGs will show new AF, 1 in 10 ECGs will be abnormal, and the reasons for this vary from benign to these which demand further examination. There are several screening types and strategies including systematic screening or ad-hoc in which patients are followed-up one single time or repeated times [5]. Screening tests may come with discomfort, lengthy waiting time for reports, false-positive results and attendant anxiety although, the early stage AF detection is beneficial for patients and cost-effective [34].

Symptomatic or asymptomatic AF has to be documented by surface ECG. The minimum duration of an ECG tracing of AF required for the diagnosis establishment of clinical AF is at least 30 seconds, or an entire 12-lead ECG [5]. Asymptomatic clinical AF has been independently related to increased risk of stroke and mortality in comparison with symptomatic AF. Data derived from studies of incidentally identified asymptomatic AF are the closest possible approximation of the risk of stroke and death in screen-detected AF subjects because delaying treatment [5]. New digital technologies for diagnosing AF has enabled the potential for innovative screening strategies. However, electrocardiograph remains

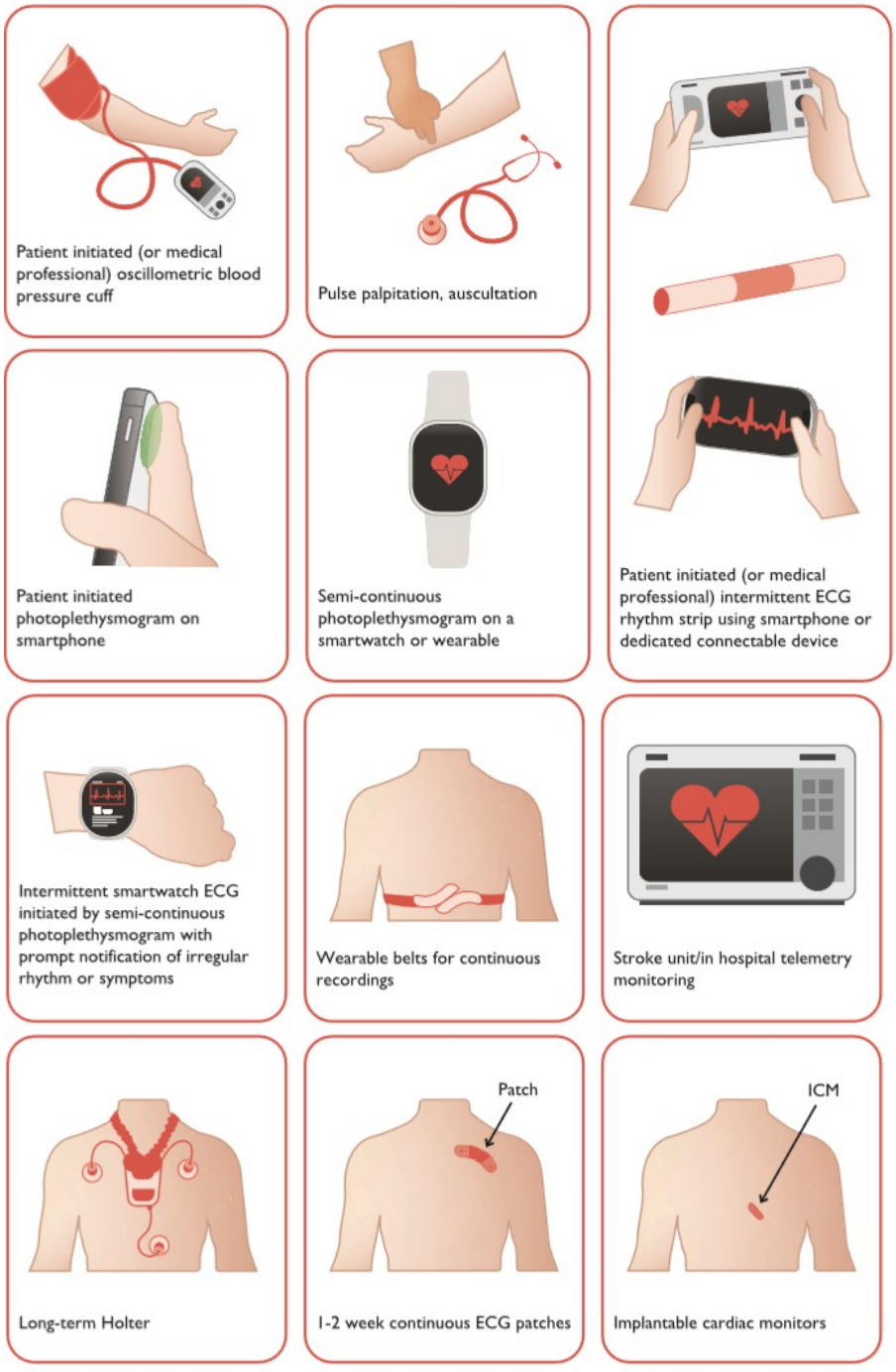

Figure 11: AF screening tools including gold standard methods as well as new mobile health technologies and implantable devices [5].

the gold standard signal used for arrhythmia detection as well as electrocardiograph-based mobile health approaches which demonstrate high accuracy [14].

Several mobile health and digital health technologies have been developed for analyzing pulse or electrocardiographic data (see Figure 11). Photoplethysmography (PPG)–based smartphone applications that allow rhythm analysis using the custom built-in camera, have been shown to detect AF with high accuracy [15]. The newest generation of smartwatches is equipped with PPG sensors and various devices, such as the Apple Watch, which have both photoplethysmograph and electrocardiograph sensors, are FDA-cleared to use electrocardiograph confirming a likely pulse irregularity identified by a photoplethysmographic signal [14].

Long-term monitoring permits the pattern assessment of AF initiation and termination, the comparison of heart rate in sinus rhythm versus AF, and the detection of asymptomatic AF. Holter monitor is a short-term recorder of 24-48h, is used to assess the ventricular rate control in patients with persistent or permanent AF. When the frequency of symptoms is sparse, the 30-day ambulatory cardiovascular telemetry monitors are another option in screening tools, documenting symptomatic transient arrhythmias. Moreover, an ambulatory ECG monitoring skin adhesive patch can be used as a 14-day recorder resulting in a higher rate of AF diagnosis [35]. However, if the initial 30-day evaluation is nondiagnostic, may need to consider an implantable loop recorder (ILR) for longer-term ECG monitoring [36].

2.6 AF management and treatment

Strategies have been developed to cope with AF including anticoagulation for stroke avoidance, better symptom control, as well as detection and management of cardiovascular risk factors. First, the identification of low-risk patients who do not need antithrombotic therapy is critical. Second, stroke prevention is another key of AF management. Common stroke risk factors are congestive heart failure, hypertension, age >75 years, diabetes mellitus, stroke, vascular disease, age 65-74 years, sex category (female) based on CHA2DS2-VASc. Non-paroxysmal AF is associated with an increase in thrombo-embolism compared with PAF. Antithrombotic therapy is initiated examining the potential risk for bleeding but non-drug options may be considered in some cases. Thus, the choice of an anticoagulant based on its effectiveness, safety and convenience [5].

Rate control is an integral part of AF management, and is often sufficient to improve AF-related symptoms. The optimal ventricular rate range is a target heart rate <80 beats per minute (bpm) at rest and <110 bpm during moderate exercise. Pharmacological rate control can be achieved with beta-blockers, digoxin, diltiazem, and verapamil, or combination therapy. However, some antiarrhythmic drugs have

rate-limiting properties and their choice depends on symptoms, comorbidities, and potential side-effects [5].

Rhythm control strategy referred to the restoration and maintenance of SR engaging a combination of treatment approaches, including cardioversion, antiarrhythmic medication, and catheter ablation, along with adequate rate control, and anticoagulation therapy. Symptomatic patients with AF can improve their QoL reducing AF-related symptoms with rhythm control. Synchronized direct current electrical cardioversion is the preferred choice in hemodynamically AF patients as it is more effective than pharmacological cardioversion resulting in immediate restoration of SR. Cardioversion is usually done by sending electric shocks to the heart through electrodes placed on the chest or with medications. Another treatment for the prevention of AF recurrences is AF catheter ablation. It is indicated to maintain the SR and improve symptoms when a patient presents paroxysmal and persistent AF in 12 months duration. Nevertheless, near of 4-14% of patients undergoing AF catheter ablation experience complications due to it is a complex procedure [5]. Cardiac ablation works by scarring or destroying tissue in the heart that triggers or sustains an abnormal heart rhythm. It uses long, flexible tubes (catheters) inserted through a vein or artery in the groin and threaded to the heart to deliver energy in the form of heat or extreme cold modifying the tissues in the heart that cause an arrhythmia.

There are five AF patterns based on presentation, duration, and spontaneous termination of AF episodes. Firstly, patients that haven't been diagnosed with AF and their symptoms are irrespective of its duration or the presence/severity. The AF that terminates spontaneously or with intervention within 7 days of onset is characterized as paroxysmal. AF that is continuously sustained beyond 7 days, including episodes terminated by cardioversion (drugs or electrical cardioversion) is referred as persistent. Furthermore, long-standing persistent is described as continuous AF of more than 12 months duration when decided to adopt a rhythm control strategy. When no further attempts to restore/maintain sinus rhythm will be undertaken it is accepted by the patient and physician as permanent AF [5].

3 Methodology

In this section, we present the study protocol, patients' demographics and we explain why vectorcardiography is a better option for clinical assessment than the standard 12-lead ECG. Also, we describe the biomedical signal processing methods that we used.

3.1 Study Protocol and Data Collection

The ECG data upon which this work is based was collected in the context of a clinical study at the 3rd Cardiology University Department at the Hippokration General Hospital, Aristotle University of Thessaloniki, Greece. The research protocol was approved by the Bioethics Committee of the Aristotle University of Thessaloniki Medical School (6229/29-7-2020). Data was collected from 82 subjects with PAF history without structural heart disease and 60 healthy subjects.

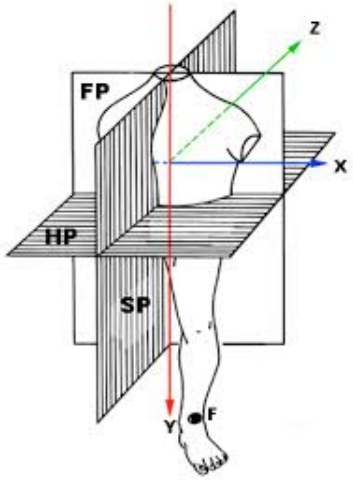

Figure 12: The three orthogonal leads and the three planes on vectorcardiography.

Orthogonal ECG recordings were obtained from a 3-channel digital recorder (GBI-3SM, Galix biomedical Instrumentation Inc. USA) at a sampling rate of 1000 Hz. The term orthogonal originates in the fact that the axes of the three planes, frontal plane (FP), sagittal plane (SP), and horizontal plane (HP) are perpendicular to each other (see Figure 12). Vectorcardiography (VCG) is the spatial representation of electromotive forces generated during cardiac activity and is analyzed in three spatial planes FP, SP, and HP. The three leads are represented by the right-left axis (X), head-to-feet axis (Y), and front-back (anteroposterior) axis (Z).

The horizontal lead from left (0°) to the right (+/–180°) is called X, the vertical lead is known as the Y orthogonal lead from down (+90°) to the top (–90°) and the axis of the sagittal orthogonal

lead known as the Z-axis, from the back (+90°) to the front (90°) (see Figure 12) [37]. VCG can also be derived from 12-leads ECG using mathematical transformations such as Kors quasi-orthogonal transformation, inverse Dower transformation, Kors regression transformation, and linear regression-based transformations [38].

The standard 12-lead ECG seemed to offer important advantages and few disadvantages as a basis for quantitative ECG analysis compared with an orthogonal lead system. VCG provides three-dimensional information of the electric activity of the atria and the ventricles and also has a greater sensitivity than the ECG in detecting atrial enlargements. In comparison with the ECG, VCG presents a greater correlation with the echocardiogram [37]. The main disadvantage of most orthogonal systems is the additional electrode placement on a patient's body that makes them less suited for ECG recording during exercise and in severely ill patients [39].

All study subjects were in the supine position for 10 minutes. Patients who presented AF, premature ventricular or atrial beats (see top Figure 10) during the ECG recording were excluded (10 patients). Lead X was used, and positive P-waves were analyzed. Thus, ECGs with negative (1 healthy subject) or biphasic P waveforms (3 PAF patients) were dismissed. This left us with a sample of 69 PAF patients and 59 healthy subjects. Table 1 shows the subjects' demographic information as well as some basic information on their average HR and number of P-waves found in their ECG recordings; the age and HR of PAF patients were statistically different from those of healthy subjects at a 0.05 significance level. There were no significant differences in the proportion of males vs females in the two groups (assessed via the two-proportion z-test at a significance level of 0.05) or in the number of P-waves present in the recordings of the two groups.

Table 1: Subjects' demographic information

	PAF n=69	Healthy n=59	P-value
Age	57.89± 10.03	55.55 ± 5.88	**0.0176**
HR	61.6±11.7	69.7± 11.3	**9.2196e-05**
P-waves	510 ±102	540 ± 103	-
Male	52 (75.36%)	38 (64.4%)	0.1763
Female	17 (24.64%)	21 (35.6%)	0.1763

3.2 Biomedical Signal Processing

In the following sections, we mention the types of ECG noise and the filters to attenuate them. We describe the P-wave electrophysiology and its morphology in the three leads as well as the process that we followed to extract P-waves. We present the ECG signal metrics and the time scaling factor that we applied to reduce HR influence.

3.2.1 ECG signal filtering

The ECG signal is contaminated by different types of noise and sometimes it heavily masked by the noise that ECG waveforms can only be revealed after appropriate signal processing. The noises can be caused by artifacts like muscle noise, power line interference, baseline wandering, and motion artifacts. Baseline wander is a low-frequency artifact in the ECG that arises due to breathing, electrically charged electrodes, or subject movement resulting in a varying isoelectric line (see Figure 13). The frequency content of baseline wander is usually below 0.5 Hz and a linear, time-invariant, highpass filter for its removal should be considered choosing carefully the cutoff frequency in order to keep the clinical information in ECG signal undistorted [40].

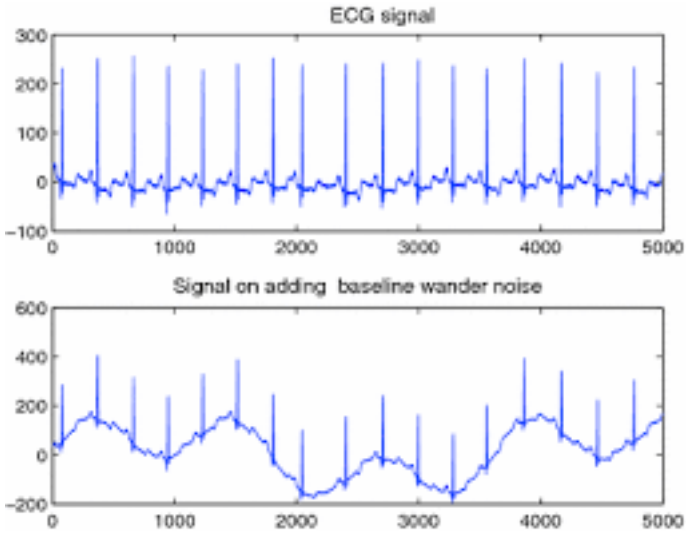

Figure 13: A clean ECG signal and at the bottom a contaminated ECG with baseline wander noise [6].

Power line interference, a common noise source introduces distortion to recorded signals and is characterized by 50 or 60 Hz sinusoidal interference. The sinusoidal component is usually a result of the use of devices that employ alternating current as a source of power because of loops in the electrical wirings, disengaged electrodes, electromagnetic interference from the power supply, improper grounding of ECG equipment, or heavy current load due to other equipment in the room [41]. Thus, delineation

of low-amplitude waveforms becomes unreliable and spurious waveforms may be introduced, negatively affecting the ECG interpretation (see Figure 14). Powerline noise is removed by low-pass filters with cut-off frequencies below 50/60 Hz or with a notch filter that can reject the transmission of frequencies within a specific frequency range and allows frequencies outside that range [40, 41].

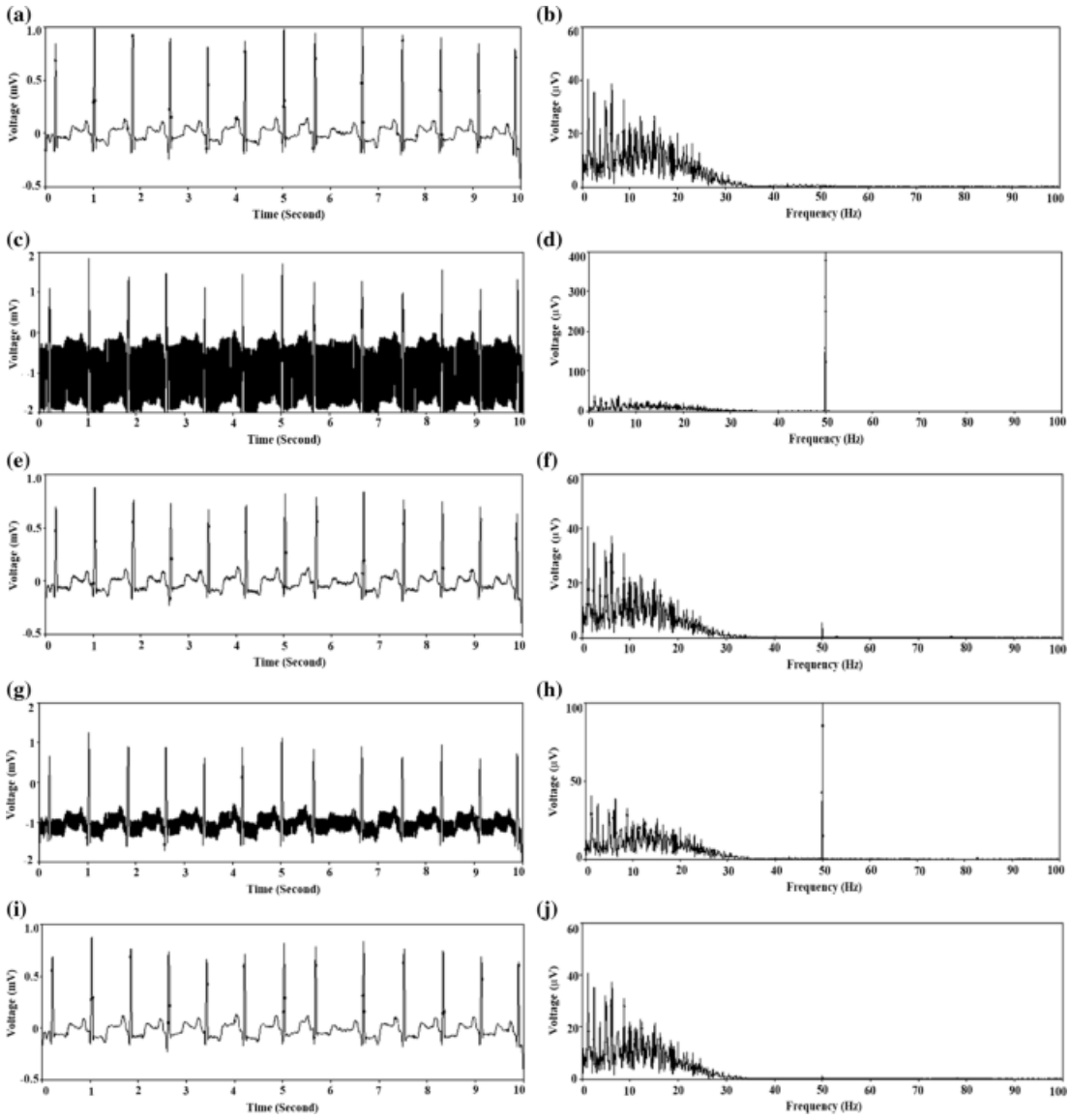

Figure 14: ECG signal (a) and its frequency spectrum (from left to right) in which at (c) and (g) was added 0.4 mV, 50 Hz powerline interface noise and 0.1 mV, 50 Hz similarly, while (e) and (i) are the ECGs after filtering [7].

Filtering is an effective way to enhance certain portions of the frequency spectrum while rejecting unwanted portions of the spectrum. For example, an ideal high pass filter with a cutoff frequency of 0.05 Hz will reject or attenuate signals with frequencies below 0.05 Hz and so will block DC voltages

(which, by definition, have a frequency of 0 Hz) but pass all frequencies above 0.05 Hz. Conversely, an ideal low pass filter with a cutoff frequency of 100 Hz will reject or attenuate all frequencies above 100 Hz while passing all frequencies from DC up to 100 Hz. In a diagnostic-quality ECG system, 50- or 60-Hz interference could be a significant problem in the pass-band, and most systems also provide an optional notch filter to reject 50 or 60 Hz. Such a notch (or band-reject) filter passes all frequencies on either side of a narrow band of frequencies centered on 50 or 60 Hz, effectively suppressing line-related noise [42].

For the purposes of this work, we are interested in isolating the P-waves present in each ECG recording. Before detecting and extracting P waveforms, all ECG signals underwent the following filtering. Baseline wander was removed using a fifth-order high-pass Butterworth filter with a cut-off frequency of 0.5 Hz. Additionally, high-frequency noise was attenuated using a fifth-order low-pass Butterworth filter with a cut-off frequency of 40 Hz. Noise due to the power line interface was removed using a notch filter at 50 Hz.

3.2.2 P-wave and its morphology

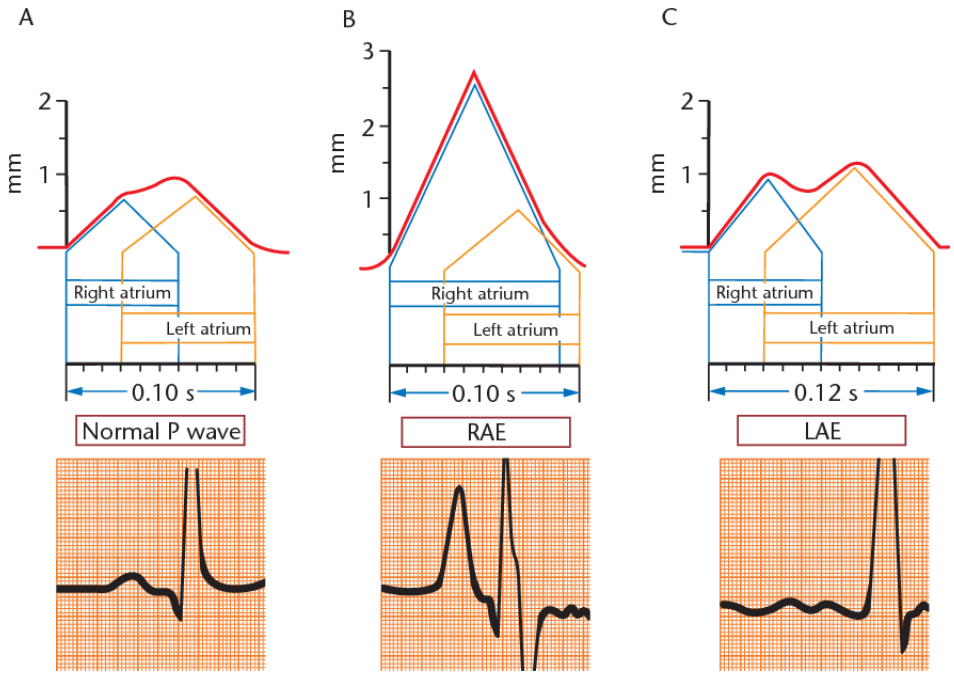

Figure 15: Schematic diagrams and corresponding ECGs of atrial depolarization in (A) normal P wave, (B) right atrial enlargement (RAE) and (C) left atrial enlargement (LAE) with interatrial conduction block [8].

The P-wave is a small deflection wave that represents atrial depolarization. It is small because the atria make a relatively small muscle mass. The P-wave is always positive in lead II under SR and may

have two humps due to the right atrium is being depolarized before the left atrium. The first half of the P-wave is a reflection of right atrial depolarization and the second half of left atrial depolarization. Atrial abnormalities as the right atrial enlargement are usually present in patients with congenital and valvular heart diseases, right atrial depolarization lasts longer than normal and its waveform extends to the end of left atrial depolarization. Additionally, left atrial enlargement is seen in patients with mitral and aortic valve disease, ischaemic heart disease, hypertension and some cardiomyopathies and left atrial depolarization lasts longer than normal but its amplitude remains unchanged (see Figure 15).

P-wave morphology reflects the projection of the depolarization vector on the ECG lead axes in three-dimensional space and covers both right and left atrial activation. It largely depends on [43]:

- origin of the SR that defines the right atrial depolarization vector.
- left atrial breakthrough that defines the left atrial depolarization vector, and
- shape and size of atrial chambers that affect the time required for completion of the depolarization process, as well as the course of depolarization wave propagation.

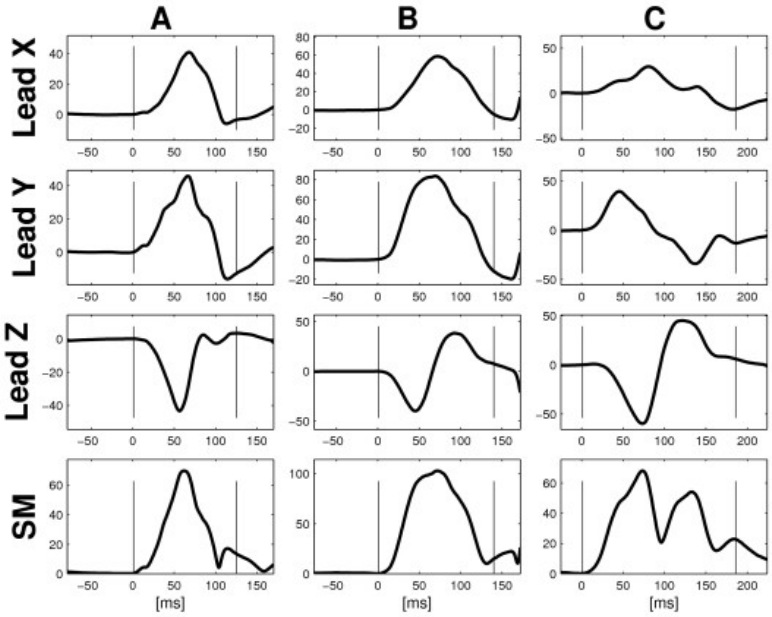

Figure 16: Types of P-wave morphology with defined P-wave limits (onset and offset); from left to right Type 1 (A), Type 2 (B), Type 3 (C) [9].

P-wave morphology can be used as a marker of conduction defect associated with arrhythmia mechanisms because appears to bear a prognostic value for prediction of clinical outcome [43]. P-waves were classified into three different types based on their morphology (see Figure 16) [9].

- Type 1: predominantly positive Leads X and Y and predominantly negative Lead Z.
- Type 2: predominantly positive Leads X and Y and biphasic Lead Z (negative, positive).
- Type 3: predominantly positive Lead X and biphasic Leads Y (positive, negative) and Z (negative, positive).
- P waves not classifiable according to these three types were denoted 'Atypical'.

3.2.3 Extracting P-waves from the ECG signal

Let $s(t)$ be the discrete-time signal corresponding to a subject's ECG recording, with $t = 0, ..., L$, L being signal length (typically $L \approx 6 \times 10^5$ for our 10min recordings at 1KHz). The Pan-Tompkins algorithm [44] was used to detect the QRS complex and R peaks in $s(t)$. A threshold on the maximum and minimum amplitude of R-peaks was used to eliminate beats which were corrupted by excessive noise due to motion artifacts. Following that, for each ECG recording, a clinical expert manually identified a single P-wave within $s(t)$ by marking its onset, t_{on}, and offset, t_{of}. That P-wave during $[t_{on}, t_{of}]$ was then used as a template to automatically identify and segment all other P-waves in the same recording using the phase-space detection algorithm from [10], which we briefly describe here.

Let $s(t)$ be a discrete-time ECG signal, and t_{ref} a given time reference point (for our purposes, t_{ref} would be either t_{on} to detect all P-wave onsets in a recording, or t_{of} for offsets). First, the algorithm generates the vectors $X(t)$ from sample differences in s:

$$X(t) = \begin{bmatrix} s(t + b_1\delta) - s(t + b_2\delta) \\ \vdots \\ s(t + b_N\delta) - s(t + b_{N+1}\delta) \end{bmatrix} \tag{1}$$

where, as per [10], we set $N = 6$, $\delta = 30$, and the vector b was $b_{on} = [0, .., N]^T$ for detecting P-wave onset and $b_{of} = [-N, .., 0]^T$ for offset. Then, the euclidean distance function

$$d(t, t_{ref}) = ||X(t) - X(t_{ref})|| \tag{2}$$

is expected to be near zero at values of t where the signal is morphologically similar to itself near t_{ref}. Thus, the onset and offset times marking the beginnings and ends of P-waves in $s(t)$ can be identified by the peaks in $d(t, t_{on})^{-1}$ and $d(t, t_{of})^{-1}$, respectively.

In practice, the distance function and its inverse can be somewhat noisy, and it was helpful to limit the

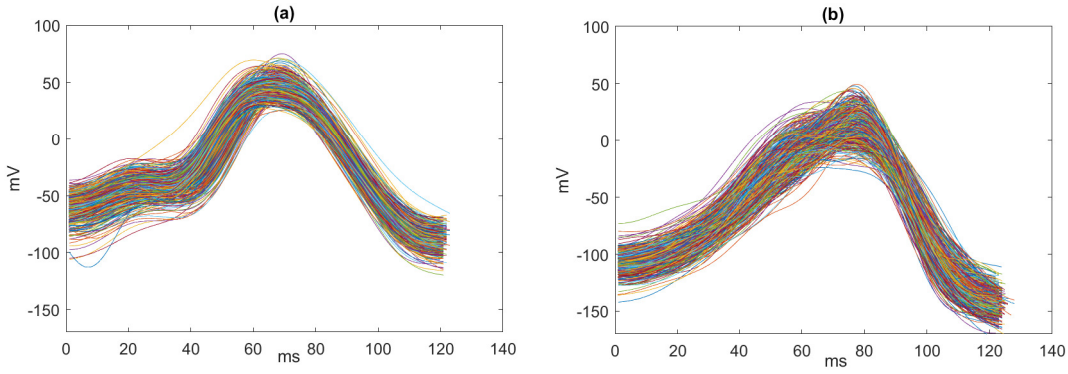

Figure 17: Characteristic examples of consecutive P-waves extracted from 10min ECG recordings Lead X, plotted over one another; (a): PAF patient, (b): Healthy

"search" for peaks of $d(t,t_{ref})^{-1}$ to intervals of t which were within reasonable distance from a cardiac cycle's R-peak - in our case we looked for inverse distance peaks within $[t_R(i)-300, t_R(i)-100]$ for onset detection (see Figure 18) and $[t_R(i)-140, t_R(i)-30]$ for offset detection, with $t_R(i)$ denoting R-peak times, measured in ms.

Also, some ECG recordings showed variations in P-wave morphology, including biphasic P waveforms which were different from the reference P-wave. Those P-waves were ignored by applying a threshold to the peaks of the inverse distance function and rejecting those peaks that were lower than the average of all peaks across the entire recording. The average number of extracted P-waves in healthy and PAF subjects was 524 ± 104. Figure 17 shows the P-waves from the ECG of a PAF patient and a healthy subject.

3.2.4 Time Scaling

P-wave duration, as well as the time between the P-wave onset and the QRS complex onset (known as the PR interval), are known to be heart rate (HR)-dependent [45] with an inverse relation [46]. For this reason, several approaches have been proposed to eliminate HR dependence effects on the PR interval and other ECG segments [46, 47]. In our case, in order to eliminate the influence of HR variations on the P-waves studied, we determined the time scaling factor that normalized each cardiac cycle in the ECG recording to a nominal 1000ms duration (equivalently, a 60 beat-per-minute HR). Thus, for the i-th P-wave extracted from the signal, we calculated a time scale coefficient of

$$a_{coef}(i) = \frac{1000}{RR_i} \tag{3}$$

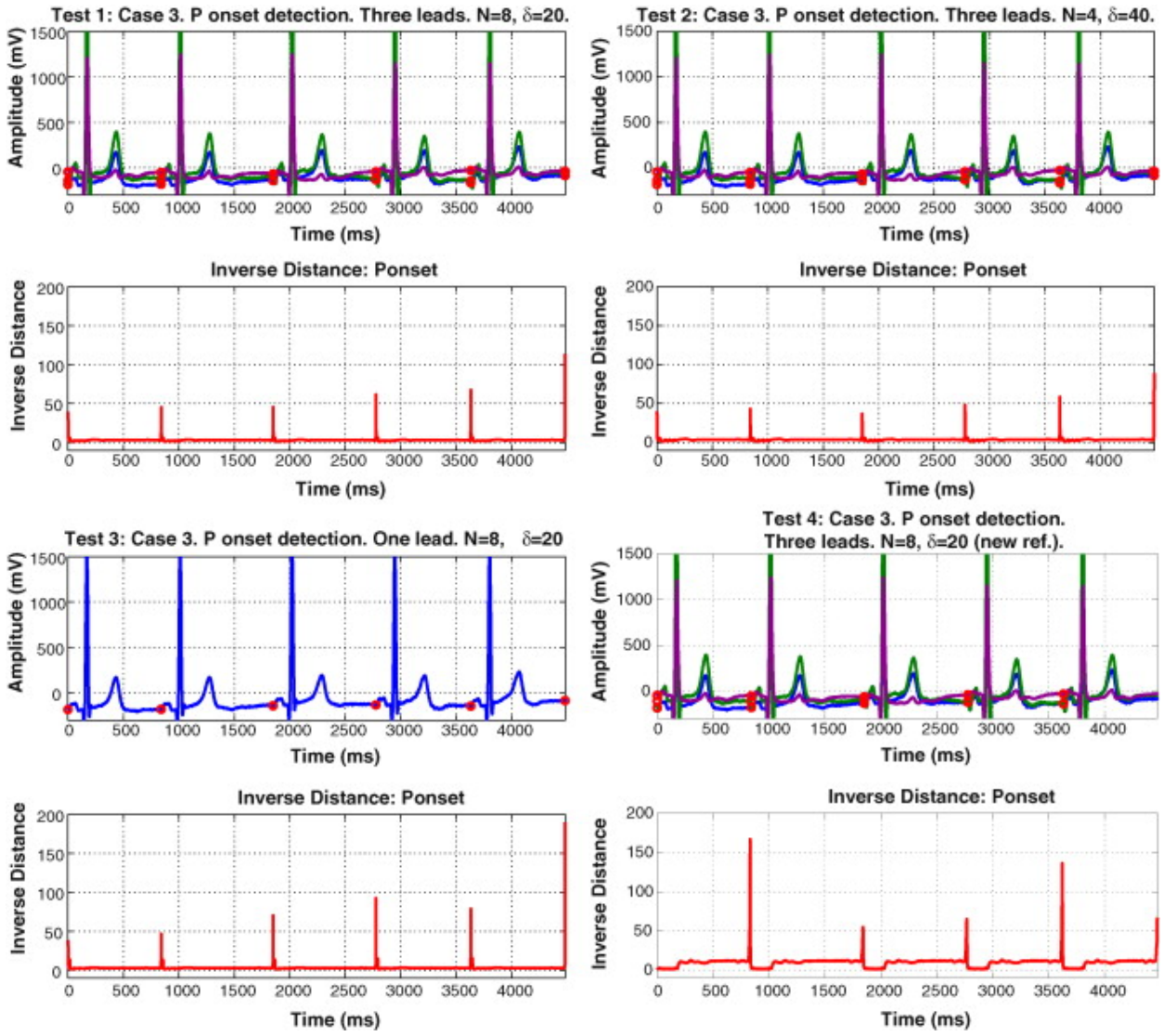

Figure 18: An illustration of P-wave onset detection using inverse distance in four different ECG signals [10].

where $RR_i = t_{R_i} - t_{R_{i-1}}$ is the time difference (in *ms*) between the i-th and the previous R-peaks. These coefficients can then be used to scale any metrics computed from the P-wave signals; for example, time scaling would imply that the amplitude of a P-wave is unaffected while its integral is scaled by a_{coef}, and its slope by a_{coef}^{-1}.

3.3 ECG Signal Metrics

The electrical depolarization of the heart's atria in each cardiac cycle was assessed through various P-wave metrics listed below. These metrics were calculated for each P-wave identified in a given recording, however, in the following we will refer to a generic P-wave signal $P(t)$, to avoid notational clutter.

- Time domain indices: these included P-wave duration P_d=t_{of}-t_{on}, the intervals $P_{on}R$=$t_R - t_{on}$ and $P_{of}R$=$t_R - t_{of}$ where t_R is the time index of the associate R-peak within the same cardiac cycle.

- P-wave amplitude, P_a, was measured as the maximum value of the ECG signal between t_{on} and t_{of}; P_a serves as an indicator of the direction of atrial depolarization and atrial myocardial mass.

- Slope-related metrics: The rate of increase of the P-wave's ascending limb was investigated at times equal to 5%, 10%, and 20% of the P-wave's duration ($t_c,\ c \in \{5\%, 10\%, 20\%\}$), measuring how quickly the P-wave rises to its maximum. These rates were given by

$$S_c = \frac{P(t_c) - P(t_{on})}{t_c - t_{on}}. \tag{4}$$

  We also computed the P-wave's maximum positive slope, S_{max} using central differences [48].

- Integral-based metrics: By considering the P-wave as a sampled version of a continuous signal, $P(\tau)$, we used Simpson's rule and the trapezoidal technique [48] to estimate

$$A = \int_{\tau_{on}}^{\tau_{of}} P(\tau) d\tau \tag{5}$$

  where $\tau_{on} = t_{on}/1000$, $\tau_{of} = t_{of}/1000$ were the continuous time counterparts of the discrete onset/offset times. We also estimated the P-wave area after shifting every P-wave so that its value at the onset, t_{on}, was zero.

$$A_0 = \int_{\tau_{on}}^{\tau_{of}} (P(\tau) - P(\tau_{on})) d\tau = A - P(\tau_{on}) P_d \tag{6}$$

- The Euclidean distance between consecutive P-waves [25] was calculated as a marker of P-wave morphological variability in each cardiac cycle:

$$D(i) = \frac{\sqrt{\sum_{t=0}^{l-1}(P_{i+1}(t_{i+1}^{on}+t) - P_i(t_i^{on}+t))^2}}{\sqrt{\sum_{t=0}^{l-1}(P_{i+1}(t_{i+1}^{on}+t))^2}} \tag{7}$$

  where $i = 1,2,...L$, L is the total number of P-waves in a recording, t_i^{on}, t_i^{of} is the onset and offset time respectively of the i P-wave, and l is the length of the shortest of the two P-waves, P_i and P_{i+1}.

The metrics listed above were calculated for each P-wave and are summarized in Table 2. They were

Table 2: P-wave features

Feature	Description
P_d	P-wave duration
$P_{on}R$	time from P onset to R peak
$P_{of}R$	time from P offset to R peak
P_a	P-wave amplitude
D	Euclidean distance between consecutive P-waves
A	P-wave area
A_0	P-wave area after offsetting P-wave to zero value at onset.
S_{max}	Max Slope
$S_{5\%,10\%,20\%}$	Slope at 5%,10%,20% of P_d

initially calculated for each identified P-wave based on the filtered ECG recordings and then adjusted to account for the time-scaling necessary to normalize all P-waves to the nominal 60bpm HR, as previously stated. In particular, a P-wave's time-domain and area metrics scale by multiplying with a_{coef}, whereas slope-related metrics are inverse proportional to the time scaling constant and thus were divided by the P-wave's a_{coef}. P-wave amplitudes and (discrete-time) euclidean distances, D, are invariant under time scaling.

4 Results

In this section, we present the tables of statistical comparison of the extracted features among healthy subjects and AF patients before and after time scaling in lead X and Y. Moreover, we demonstrate the classification results testing various feature selection methods.

4.1 Statistical Data Analysis

We performed means testing to eliminate features which showed no statistically significant differences between the two groups (PAF vs. healthy), in order to avoid redundancy [49, 50]. The normality of each feature's distribution in either group was assessed with the Lilliefors test. To detect statistically significant differences in feature means between PAF and healthy subjects we used the two-sample t-test in the cases where both samples were normally distributed and the non-parametric Wilcoxon signed rank-sum test in all other cases. A significance level of 0.05 was chosen for all testing.

4.1.1 ECG lead X

We examined the statistical differences of X lead features among PAF patients and healthy controls in the case of applying time scaling and without scale (Table 3-Table 12). We observed that the mean values of P-wave areas A, A_0 averaged over a subject's recordings, as well as ΔA; the means of S_{max} were significantly different with and without time scaling except $P_{of}R$; while the standard deviations of $P_{on}R, P_{of}R$ as well as all slope-related features; S_{max}, $S_{5\%}$, $S_{10\%}$, $S_{20\%}$ demonstrated in both approaches significant differences. The coefficient of variability and the maximum value (over each subject's entire recording) of time-domain indices $P_{on}R, P_{of}R$ also the areas features A, A_o, and S_{max} was significantly different in PAF subjects compared to the healthy controls in all cases as well as the minima of $P_{of}R$, ΔA and S_{max}. Finally, all descriptive statistics of invariable of time scale D except its minimum value within a subject's recording were significantly different among the two groups. The P_d was mostly significant different between the groups after time scale except for its maximum value.

Table 3: Mean value ± SD of *mean* P wave features without ts.

Features	AF	Healthy	*p*-Value
$P_{of}R$	86.2329± 21.5761	84.8570± 19.8760	0.8559
A	-1.3959e+03 ± 2.6536e+03	-4.8193e+03 ± 5.1021e+03	**1.4534e-05**
A_0	3.1421e+03± 1.2542e+03	5.5438e+03 ± 3.4012e+03	**6.6472e-07**
ΔA	4444 ± 2.8177e+03	1.0357e+04 ± 6.5584e+03	**3.2779e-08**
S_{max}	3.0939 ± 1.7063	4.3423 ± 2.3548	**4.9930e-06**
D	0.4806 ± 0.6035	0.1897 ± 0.1258	**4.7527e-04**

Table 4: Mean value ± SD of *cv* P-wave features without ts.

Features	AF	Healthy	*p*-Value
P_d	0.0454 ± 0.0453	0.0301 ± 0.0164	0.1731
$P_{on}R$	0.0194 ± 0.0226	0.0131 ± 0.0219	**0.0275**
$P_{of}R$	0.0713 ± 0.0580	0.0467 ±0.0489	**0.0012**
A	-1.2150 ±7.4185	-0.3548 ± 0.5764	**0.0403**
A_0	0.4103 ± 0.3792	0.1670 ± 0.3259	**1.3379e-04**
ΔA	0.1983 ± 0.1293	1.0515 ±3.7167	**7.7261e-11**
D	4.0631 ± 3.5813	1.1779 ± 0.7356	**4.7527e-04**
S_{max}	0.2197 ± 0.1764	0.1966 ± 0.0443	**0.0076**

Table 5: Mean value ± SD of *std* P-wave features without ts.

Features	AF	Healthy	*p*-Value
$S_{20}\%$	0.3501 ±0.3009	0.5168 ± 0.3284	**5.9355e-05**
ΔA	2.0912e+03 ± 1.8107e+03	1.7089e+03 ± 1.0340e+03	0.7451
P_d	5.2982 ± 5.7110	3.3039 ±1.6992	0.0657
$P_{on}R$	4.1552 ± 5.0321	2.6706 ±4.5869	**0.0282**
$P_{of}R$	5.8920 ± 4.4740	3.8465 ±4.3047	**6.7703e-04**
S_{max}	0.7668 ± 1.1430	0.8512 ±0.4681	**1.1428e-05**
$S_{5\%}$	0.4665 ±0.3180	0.6531 ± 0.4441	**0.0020**
$S_{10\%}$	0.4374 ± 0.3262	0.6294 ± 0.4194	**4.9258e-04**
D	3.1965 ± 5.9488	0.2825 ± 0.4028	**9.3217e-08**

Table 6: Mean value ± SD of *MAX* P-wave features without ts.

Features	AF	Healthy	*p*-Value
P_d	146.4638 ± 43.7938	124± 17.6098	**0.0027**
P_a	156.0968± 194.2390	91.6108 ± 70.1734	**0.0247**
$P_{on}R$	226.2754 ± 47.6818	215.7458 ± 103.6740	**0.0208**
$P_{of}R$	106.8841 ± 26.2284	106.7458 ± 99.7918	**0.0090**
A	1.3511e+04 ± 2.7100e+04	1.0764e+03 ± 5.3832e+03	**8.6246e-10**
A_o	8.9997e+03 ±	1.0541e+04 9.1240e+03± 5.0056e+03	**0.0068**
ΔA	2.1614e+04 ± 3.1507e+04	1.6764e+04 ± 9.3884e+03	**0.0095**
S_{max}	6.1391± 5.2269	7.6604 ± 4.2786	**2.0002e-04**
D	67.5864 ± 142.1683	4.0997 ± 8.0911	**5.6415e-09**

Table 7: Mean value ± sd of *MIN* P-wave features without ts.

Features	AF	Healthy	*p*-Value
P_d	101.2609 ± 27.2190	104.1695 ± 18.5715	0.7056
$P_{on}R$	195.3913 ±26.5625	191.7288 ± 23.2563	0.2502
$P_{of}R$	106.8841 ± 26.2284	106.7458 ± 99.7918	**0.0090**
A_0	-2.4343e+03 ±8.1567e+03	2.1466e+03 ± 2.5583e+03	**2.7664e-07**
ΔA	-1.0748e+04 ± 2.2104e+04	4.0962e+03± 5.7395e+03	**3.8182e-14**
S_{max}	1.5153 ± 0.8676	2.3529 ± 1.3731	**2.4332e-05**

4.1.2 ECG lead X time scaling

We observed higher mean values in A_o, $P_{of}R$, ΔA, S_{max} in healthy subjects compared with PAF patients whereas A and D present lower values, respectively. The coefficient of variability and standard deviation of time-domain features and D were significantly higher in AF patients while the standard deviation of slope features except S_{max} demonstrated greater variation in healthy controls. We found greater values in maximum, minimum, and coefficient of variation of area features in healthy subjects excluding the maximum of ΔA and D. Moreover, time-domain features in their maximum values were significantly higher in PAF patients whereas were lower in their minimum values except $P_{on}R$ compared with healthy subjects.

Table 8: Mean value ± SD of *mean* P-wave features with time scaling (ts).

Features	AF ts	Healthy ts	*p*-Value
$P_{of}R$	88.9113 ± 24.4752	97.4587 ± 24.4159	**0.0262**
A	-1.4732e+03± 2.8130e+03	-5.6243e+03 ± 6.8123e+03	**9.7935e-06**
A_0	3.2971e+03 ± 1.4955e+03	6.7979e+03± 4.3382e+03	**4.9192e-08**
ΔA	4767±3125	12237±8567	**9.4114e-09**
S_{max}	2.9914 ± 1.4787	3.8919 ± 2.0271	**4.5521e-05**
D	0.4806 ± 0.6035	0.1897 ± 0.1258	**4.7527e-04**

Table 9: Mean value ± SD of *cv* P-wave features with time scaling (ts).

Features	AF ts	Healthy ts	*p*-Value
P_d	0.1032 ± 0.0637	0.0554± 0.0232	**1.0088e-07**
$P_{on}R$	0.0848± 0.0487	0.0456 ± 0.0340	**1.6943e-08**
$P_{of}R$	0.1038 ± 0.0653	0.0628 ± 0.0618	**3.0620e-07**
A	-0.2706± 8.7600	-0.3448± 0.5844	**0.0256**
A_0	0.4454± 0.4106	0.1709 ± 0.3284	**6.5526e-06**
ΔA	-1.2735± 16.2740	0.2157±0.1296	**1.0947e-10**
D	4.0631 ± 3.5813	1.1779 ± 0.7356	**4.7527e-04**
S_{max}	0.2600± 0.2419	0.2007 ± 0.0477	0.1031

Table 10: Mean value ± SD of *std* P-wave features with time scaling (ts).

Features	AF ts	Healthy ts	*p*-Value
$S_{20}\%$	0.3533 ±0.2510	0.4593± 0.2845	**0.0013**
ΔA	2568±2737	2229±1477	0.1855
P_d	13.3858 ± 10.7836	7.1725 ±3.2003	**1.4853e-05**
$P_{on}R$	18.4974 ± 12.5883	10.2100 ± 8.0506	**1.3464e-06**
$P_{of}R$	9.1021 ± 6.0537	5.9244 ± 6.3464	**2.0963e-05**
S_{max}	0.8123 ± 1.0348	0.7754 ± 0.4073	**3.6910e-04**
$S_{5\%}$	0.4582± 0.2623	0.5796 ± 0.3850	**0.0168**
$S_{10\%}$	0.4323± 0.2653	0.5575 ± 0.2653	**0.0062**
D	3.1965 ± 5.9488	0.2825 ± 0.4028	**9.3217e-08**

Table 11: Mean value ± sd of *MAX* P-wave feature with time scaling (ts).

Features	AF ts	Healthy ts	*p*-Value
P_d	214.8409 ± 100.5322	155.9195 ±32.2268	**4.9257e-04**
P_a	156.0968 ± 194.2390	91.6108 ± 70.1734	**0.0247**
$P_{on}R$	338.3186 ± 123.2980	276.5032 ± 137.9361	**3.8277e-04**
$P_{of}R$	145.0143 ± 55.7775	130.9679 ± 131.1215	**9.5982e-07**
A	1.4698e+04± 2.6264e+04	1.5807e+03 ± 6.6700e+03	**1.5587e-08**
A_0	1.0726e+04 ± 1.1217e+04	1.1399e+04 ± 6.6919e+03	**0.0286**
ΔA	29038±56170	20743±13004	**0.0398**
S_{max}	7.8027± 8.8642	6.9737 ± 3.7043	**0.0148**
D	67.5864 ± 142.1683	4.0997 ± 8.0911	**5.6415e-09**

Table 12: Mean value ± sd of *MIN* P-wave features with time scaling (ts).

Features	AF ts	Healthy ts	*p*-Value
P_d	81.2565 ± 28.0967	107.4689 ± 27.6779	**7.5171e-07**
$P_{on}R$	144.6147 ± 45.3702	189.6509 ± 44.2447	**1.5928e-07**
$P_{of}R$	145.0143 ± 55.7775	130.9679 ± 131.1215	**0.0051**
A_0	-3.1100e+03± 8.3540e+03	2.4453e+03 ± 2.9555e+03	**6.0959e-08**
ΔA	-11538±19614	45787±69699	**7.6897e-15**
S_{max}	1.3715 ± 0.8308	2.0967 ± 1.2307	**2.2829e-05**

4.1.3 ECG lead Y

We examined the statistical differences of Y lead features among PAF patients and healthy controls in the case of applying time scaling and without scale (Table 13-Table 22). The results from lead Y have shown that the mean values of areas A_0, S_{max} present statistical differences before and after time scaling except $P_{on}R$ that is significantly different only in time scaling. The coefficient of variation values of time-domain features P_d,$P_{on}R$, $P_{of}R$ were significantly different after time scaling while euclidean distance D and S_{max} before and after scale. Although, we observed that the standard deviation of time-domain indices demonstrated differences among the cohorts only with time scaling whereas S_{max} and $S_{20\%}$ in both conditions. Additionally, maximum (over each subject's entire recording) values of S_{max}, $S_{20\%}$ present statistically differences before scaling but P_d after scaling, although time-domain features $P_{on}R$, $P_{of}R$, D in both approaches. Minima values of time-domain were significantly different only in time scaling while areas A_0 and S_{max} in both approaches.

Table 13: Mean value ± SD of *mean* P-wave features without ts.

Features	AF	Healthy	*p*-Value
$P_{on}R$	217.5250 ± 34.3891	208.2968 ± 26.4289	0.1261
A_0	4.5355e+03± 2.3436e+03	6.5105e+03 ± 4.5199e+03	**0.0049**
S_{max}	3.6570± 1.8313	4.4188 ± 2.4467	**0.0020**

Table 14: Mean value ± SD of *cv* P-wave features without ts.

Features	AF	Healthy	*p*-Value
P_d	0.0394 ± 0.0416	0.0360 ± 0.0294	0.3714
$P_{on}R$	0.0200 ± 0.0178	0.0142 ±0.0086	0.2474
$P_{of}R$	0.0716 ± 0.0774	0.0484 ± 0.0250	0.8409
D	3.6316 ± 4.0722	2.0632 ± 3.4423	**4.4540e-06**
S_{max}	0.1946 ± 0.1365	0.2021 ± 0.0736	**0.0087**

Table 15: Mean value ± SD of *std* P-wave features without ts.

Features	AF	Healthy	*p*-Value
$S_{20\%}$	0.4324± 0.3732	0.5642 ± 0.3721	**0.0050**
P_d	4.8918 ± 5.2535	4.1334 ± 2.7559	0.4646
$P_{on}R$	4.4536 ± 4.0634	3.0836 ± 1.9837	0.1823
$P_{of}R$	5.7010 ± 5.5043	4.1312 ± 2.3123	0.6497
S_{max}	0.7792 ± 1.1064	0.8795 ± 0.4808	**1.6855e-04**
$S_{5\%}$	0.6758 ± 0.7138	0.7566 ± 0.4677	**0.0253**
$S_{10\%}$	0.6089± 0.5924	1.3385 ± 5.4355	0.0879

Table 16: Mean value ± sd of *MAX* P-wave features without ts.

Features	AF	Healthy	*p*-Value
$S_{20\%}$	3.4056± 3.0033	3.6621 ± 2.2216	**0.0354**
P_d	149.5072 ± 37.6769	137.5424 ± 22.6261	0.0852
$P_{on}R$	237.6812 ± 44.2674	219.2034 ± 32.4238	**0.0196**
$P_{of}R$	110.1449 ± 27.1224	98.3051 ±23.1571	**0.0099**
A	1.4241e+04 ± 2.1229e+04	4.3067e+03± 7.6198e+03	**2.6013e-04**
S_{max}	11.9616 ± 8.2407	4.6358 ± 4.2786	**0.0075**
D	269.8619± 1.7563e+03	315.4555 ± 1.9564e+03	**0.0075**

Table 17: Mean value ± sd of *MIN* P-wave features without ts.

Features	AF	Healthy	*p*-Value
P_d	111.0580± 29.6692	110.6271 ± 25.4300	0.7889
$P_{on}R$	203.7246 ± 31.2776	198.9661 ± 22.9031	0.4500
$P_{of}R$	70.6377 ± 27.1975	73.4576 ± 18.1444	0.3317
A_0	-2.6888e+03 ± 1.1084e+04	2.0721e+03± 3.7574e+03	**0.0036**
S_{max}	1.9870 ± 0.9180	2.4846 ± 1.5802	**0.0096**

4.1.4 ECG lead Y time scaling

We observed higher mean values in A_o, $P_{on}R$ and S_{max} in healthy subjects compared with PAF patients. The coefficient of variability and standard deviation of time-domain features and D were significantly higher in AF patients whereas in slope features were lower, respectively. Time-domain features in their maximum values were significantly higher in PAF patients while their minimum values were lower. However, the slope features, D, and area A_o exhibited greater values in healthy controls in their minima and maxima measures.

Table 18: Mean value ± SD of *mean* P-wave features with time scaling (ts).

Features	AF ts	Healthy ts	*p*-Value
$P_{on}R$	226.0374 ± 47.1612	241.8999 ± 44.5522	**0.0334**
A_0	4.8847e+03 ± 2.7355e+03	7.6457e+03 ± 5.4659e+03	**0.0031**
S_{max}	3.5494 ± 1.6552	4.0465 ± 2.6949	**0.0427**

Table 19: Mean value ± SD of *cv* P-wave features with time scaling (ts).

Features	AF ts	Healthy ts	*p*-Value
P_d	0.1056 ± 0.0916	0.0608 ± 0.0341	**4.5521e-05**
$P_{on}R$	0.0944 ± 0.0809	0.0473± 0.0287	**1.4173e-07**
$P_{of}R$	0.1208 ± 0.1128	0.0664 ± 0.0386	**4.1155e-04**
D	3.6316 ± 4.0722	2.0632 ± 3.4423	**4.4540e-06**
S_{max}	0.2290 ± 0.1965	0.3663 ± 1.1263	**0.0447**

Table 20: Mean value ± SD of *std* P-wave features with time scaling (ts).

Features	AF ts	Healthy ts	*p*-Value
$S_{20\%}$	0.4773 ± 0.5037	1.7602 ± 9.6611	**0.0484**
P_d	14.7242 ± 14.7309	8.2360 ±3.8585	**0.0016**
$P_{on}R$	21.6308 ± 20.5772	11.1338 ± 6.2575	**5.9870e-06**
$P_{of}R$	10.5051 ± 10.0120	6.2888 ± 3.1731	**0.0032**
S_{max}	0.8780 ± 1.1933	3.2295 ± 18.5377	**0.0126**
$S_{5\%}$	0.6530± 0.6657	1.2536 ± 4.5482	0.0630
$S_{10\%}$	0.6089± 0.5924	1.3385 ± 5.4355	0.0879

Table 21: Mean value ± sd of *MAX* P-wave features with time scaling (ts).

Features	AF ts	Healthy ts	*p*-Value
$S_{20\%}$	4.4299 ± 8.2992	18.2869 ±114.3946	0.4973
P_d	229.6661 ± 145.2694	171.7274± 35.1672	**0.0484**
$P_{on}R$	370.5986 ± 211.1127	278.0345 ± 46.7135	**0.0042**
$P_{of}R$	157.7082 ± 101.8461	119.8967 ± 27.3260	**0.0092**
A	1.9759e+04±4.0707e+04	4.7998e+03 ± 8.5367e+03	**5.1047e-04**
S_{max}	10.0339± 17.2777	36.3337 ± 219.2835	0.1093
D	269.8619± 1.7563e+03	315.4555 ± 1.9564e+03	**0.0075**

Table 22: Mean value ± sd of *MIN* P-wave features with time scaling (ts).

Features	AF ts	Healthy ts	*p*-Value
P_d	89.0272 ± 33.0270	110.7652 ± 41.8538	**3.6910e-04**
$P_{on}R$	156.0954 ± 49.6278	193.5994 ± 61.2292	**2.7046e-05**
$P_{of}R$	58.4368 ±24.9536	75.9448 ± 28.5200	**2.3255e-04**
A_0	-3.5962e+03 ± 1.4350e+04	2.3054e+03 ± 4.1018e+03	**0.0012**
S_{max}	1.7277 ± 0.8297	2.1002 ± 1.3271	**0.0359**

4.2 Feature Selection methods and Classification

In the following section, we report the feature selection methods that we used to reduce feature space dimension, presenting the feature vectors as well as their classification results using Random Forests.

4.2.1 Feature selection process

Feature selection methods are useful for obtaining a lower-dimensional feature space (FS) by removing irrelevant and redundant features from the data. The main goal of these methods is to find a subset of features that can build a robust predictor defying the curse of dimensionality. We extracted sixty features as they were presented in Table 28 and we applied a pre-processing step such as filter methods [49, 50] as an intrinsic criterion. Filter methods utilize univariate and multivariate techniques as t-test, Wilcoxon rank-sum, X square, correlation. To avoid redundancy, we excluded features with a p-value above 0.05 based on the Wilcoxon rank-sum test for the nonparametric distributions of PAF and healthy subjects. Thus, 34 features were selected for further examination.

We considered the Feature Importance (FI) index to select the most contributing features. Initially, a feature vector (FV) consisted of 34 features was tested as an input to Random Forest (RF). We applied 10-fold validation and in each fold we noted the less important feature through a score, repeating this process 10 times. Afterward, the feature with the lowest score was removed from input vector and the reduced one participated in a new classification task. All feature combinations via this procedure were checked, tracking the most important feature which finally remained in the last FV.

Further, we evaluated another method, the max volume (MV) concept [51]. In a given matrix nxm (dataset), the n rows represent the observations and m columns the features. We seek a subset of k features that are linear independent to reduce the dimension of the features (k$<$ m). We calculated the determinant in all possible combinations of subsets, searching for its maximum value k in order to reconstruct the matrix using only a few columns, thus having a more compact representation of data.

The overlap of confidence interval (OCI) is examined as an additional technique for selecting a subset of features. Between two distributions we seek a measure of an agreement to assess the similarity of two populations [52]. We computed the sample mean and standard error determining the 95% confidence interval for each population mean. Then we measured the overlap between them [53], selecting a feature with the minimum OCI among PAF patients and healthy.

The singular value decomposition (SVD) might be the most popular technique for dimensionality reduction. Any matrix A of rank r can be written as A=USV^T where U and V are orthogonal matrices (square matrices whose columns form an orthonormal basis) and S is a diagonal matrix (a matrix whose

only non-zero entries lie along the diagonal). The diagonal entries s_i are called singular values which are always positive or 0. It is possible to exactly represent A using the reduced SVD of rank k as its best approximation. High singular values correspond to dimensions of the new space where examples have more variability whereas low singular values determine dimensions where examples have a smaller variability [54] . The conditional number is the ratio C of the largest to smallest singular value in the SVD of a matrix. Values of C near 1 indicate a well-conditioned matrix, and large values of C indicate an ill-conditioned matrix.

The determinant (DET) of a square matrix quantifies how that matrix changes the volume of a unit hypercube. The absolute value of the determinant of a square matrix A is equal to the product of its singular values. The basic idea is that the important information in a matrix is really contained in its largest singular values, and one may often ignore the smaller singular values without losing the essential features of the data.

A total of 60 features were examined for this study in which 34 of them present statistical differences. However, we restricted the FS using only 15 features, excluding the time-domain features due to MV, OCI, SVD, and DET are time-consuming methods.

4.2.2 Classification Procedure

The Random Forest classification model with an ensemble of 20 grown trees was used to discriminate between PAF patients and healthy subjects. Random Forest is a classifier that combines individuals decision trees to predict a class based on the majority vote of the predictions of all trees [55]. The data that is not used to build the current tree is known as out-of-bag error (OOB) sample. The prediction error is measured on the OOB sample for quantifying FI. FI is a technique that permits a better understanding of the model by indicating the features which contribute the most to the decision-making.

Table 23: Classification metrics

Measure	Form
ACCURACY	ACC=(TP+TN)/(TP+TN+FP+FN)
SENSITIVITY	SE=TP/(TP+FN)
SPECIFICITY	SP=TN/(FP+TN)

TP:true positive, TN:true negative, FP:false positive, FN:false negative

The effectiveness of model performance was evaluated using 10-fold cross-validation ensuring low bias and variance. In 10-fold cross-validation the data D is split into 10 subsets D_i i=1,..,10 of equal size.

Then the classifier is trained and tested 10-times using all folds as a training set except one D_i every time that is used as a test set [56]. To obtain more robust classification results, each cross-validation scheme was repeated 10 times, i.e., 100 iterations of the classification process. Classification performance indices were measured such as the average accuracy (ACC), sensitivity (SE), and specificity (SP) of the individually 10-folds in the 10 repetitions for each test set. Metrics of performance are described in Table 23 [57]. The statistical analysis and Random Forest classification were implemented using Matlab R2018b (Mathworks Inc., Natick, MA, USA).

Classification results using features after time scaling of lead X are demonstrated in Tables 24-27 and Tables 30-31 using OOB, MV, and OCI feature selection methods. In particular, in Table 24 ten FVs are presented based on feature importance starting with 34 features as initial FV.

Table 24: Classification results based on OOB method

Feature Sets	ACC	SE	SP
$[\ \mu A_0]$	81.27 $\pm$ 2.80	78.38 $\pm$2.68	84.56$\pm$ 3.32
$[\mu A_0, cvD]$	88.51 $\pm$1.59	89.26 $\pm$3.09	87.56$\pm$ 4.68
$[\ \mu A_0, cvD, stdS_{max}]$	88.38 $\pm$ 1.99	89.90 $\pm$ 2.15	86.73$\pm$ 5.26
$[\mu A_0, cvD, stdS_{20\%}, stdS_{max}]$	92.34 $\pm$ 1.49	94.47 $\pm$2.94	89.83$\pm$ 3.10
$[\mu A_0, cvD, stdS_{20\%}, stdS_{max}, cvP_d]$	91.42 $\pm$1.71	93.64 $\pm$ 2.46	88.90$\pm$ 3.99
$[\mu A_0, cvS_{max}, cvD$ $stdS_{20\%}, stdS_{max}, cvP_d\ ]$	93.07 $\pm$2.01	94.81 $\pm$ 4.66	91.03$\pm$ 3.48
$[\mu A_0, cvS_{max}, cvDstdS_{20\%}$ $stdS_{max}, maxA, cvP_d\ ]$	**92.85** $\pm$ 1.90	93.78 $\pm$ 3.53	91.80$\pm$4.03
$[\mu A, \mu A_0, cvS_{max}, cvD$ $stdS_{20\%}, stdS_{max}, maxA, cvP_d]$	92.14 $\pm$ 2.07	93.33 $\pm$ 1.77	90.73$\pm$ 4.69
$[\mu A, \mu A_0, cvS_{max}, cvD$ $stdS_{20\%}, stdS_{max}, maxA, minS_{max}, cvP_d]$	**93.70** $\pm$ 1.10	95.26 $\pm$ 2.00	91.86$\pm$ 3.82
$[\mu A, \mu A_0, cvS_{max}, cvD, stdS_{20\%}$ $stdS_{max}, maxA, minS_{max}, cvP_d, minPonR]$	**93.67** $\pm$ 1.76	94.38 $\pm$ 3.57	94.86$\pm$ 3.62

Table 25: Classification results based on MV

Feature Sets	ACC	SE	SP
[μA, μA_0, mD, cvA, cvA_0, cvS_{max},cvD, $stdS_{max}$,$stdS_{10\%}$, $maxA$]	**92.97 ±1.87**	**94.19±2.33**	**91.63 ±3.67**
[$\mu A, \mu A_0, cvA, cvA_0, cvS_{max}$, $cvD, stdS_{max}, stdD, maxA$]	92.8 ±1.06	93.79±2.07	91.67 ±2.98
[μA, μA_0, cvA, cvA_0, $stdS_{max}$, $stdS_{10\%}$,$stdD$,$maxA$]	92.45 ±2.24	92.98±3.91	91.73 ±3.26
[μA, μA_0, cvA, cvA_0,$stdS_{max}$,$stdD$,$maxA$]	90.17 ±2.00	89.93±3.67	90.37 ±3.06
[μA, μA_0, cvA, $stdS_{max}$,$stdD$,$maxA$]	89.19 ±1.55	87.17±2.61	91.50 ±3.40
[μA, cvA,$stdS_{max}$,$stdD$,$maxA$]	88.87 ±1.33	86.29±2.87	91.87 ±3.67
[μA, cvA, $stdD$, $maxA$]	82.2 ±3.16	83.48±2.85	80.73 ±4.21
[μA, cvA, $maxA$]	81.83 ±2.41	82.33±2.66	81.33 ±3.42
[μA, $stdD$]	77.54 ±1.94	78.76±2.91	76.17 ±2.36

Tables 25-26 show the classification performance of 10 FVs consisted of features that are selected based on MV and OCI methods. Table 30 summarizes high performance FVs of different lengths on the previously referred feature selection methods.

A new feature $\Delta A = A_0 - A$ was added in the initial FV and the maximum classification results are depicted in Table 27. The highest classification metrics were achieved using 5 features of P-wave integral and slope. In Table 31 the best FV is presented plus the effects of adding a sixth feature, the next in order of importance or removing the least important of the five features. However, classification results of lead Y show low performance after testing all feature selection methods, and only the FVs with the highest performance are illustrated in Table 32.

Table 26: Classification results based on OCI

Feature Sets	ACC	SE	SP
$[\mu A, \mu A_0, \mu S_{max}, \mu D, cvA, cvA_0,$ $stdS_{20\%}, stdS_{max}, stdS_{5\%}, stdS_{10\%}$]	92.00 ± 2.20	93.00± 4.24	90.73± 3.38
$[\mu A, \mu A_0, \mu S_{max}, \mu D, cvA,$ $stdS_{20\%}, stdS_{max}, stdS_{5\%}, stdS_{10\%}]$	**93.22 ± 2.52**	**93.81± 3.37**	**92.47± 3.91**
$[\mu A,\ \mu A_0,\ \mu S_{max},$ $cvA,\ stdS_{20\%},\ stdS_{max}, stdS_{5\%}, stdS_{10\%}$]	93.01 ± 3.07	94.19± 3.37	91.53± 3.98
$[\mu A,\ \mu A_p,\ cvA,$ $stdS_{20\%},\ stdS_{max}, stdS_{5\%}, stdS_{10\%}$]	92.63 ± 1.75	93.36± 3.52	91.87± 4.48
$[\mu A,\ cvA,\ stdS_{20\%},$ $stdS_{max}, stdS_{5\%}, stdS_{10\%}$]	89.43 ± 2.04	87.83± 4.23	91.3± 3.87
$[\ cvA,\ stdS_{20\%},\ stdS_{max},$ $stdS_{5\%}, stdS_{10\%}$]	85.6 ± 2.75	85.62± 2.87	85.57± 3.66
$[\ cvA,\ stdS_{max}, stdS_{5\%}, stdS_{10\%}$]	86.1 ± 1.38	87.64± 3.07	84.13± 4.28
$[\ cvA,\ stdS_{max}, stdS_{5\%}]$	85.87 ± 1.82	86.55± 3.49	85.07± 4.45
$[\ cvA,\ stdS_{max}]$	85.31 ± 2.71	85.52± 4.56	85.13± 4.45

Table 27: Classification results with a new added feature ΔA

Method	Feature Sets	ACC	SE	SP
OOB	$[\mu\Delta A, \sigma S_{20\%}, \sigma S_{max}, minA, minS_{max}]$	**95.01 ± 0.91**	**95.47 ± 2.03**	**94.43±3.56**
OCI	$[\ \sigma S_{max},\ cv\Delta A\ , maxA\ maxS_{max},\ cvA]$	87.87 ± 2.04	90.05± 2.25	85.50± 4.38
MV	$[\ cv\Delta A,\ \mu A,\ \max P_a\ , maxD,\ maxA]$	81.92 ±2.65	83.19±2.21	80.50 ±3.36

5 Discussion

In this section, we discuss the results of statistical analysis, as well as the classification results reporting the applicability of the time scaling factor and the superiority of lead X versus Y. Besides, we briefly review the state of the art works compared to our method.

5.1 Results Discussion

In this study, we investigated beat-to-beat P-waves taken from 10-minute long ECG in lead X and Y during the SR of 69 PAF patients and 59 healthy subjects, eliminating heart rate influence. We focused on common P-wave measures such as P duration, P area and we introduce P-wave slope and ΔA area as novel indices. We show that significant differences exist among the groups before and after time scaling in P-wave features. Moreover, we examined five methods of feature selection due to the plethora of extracted features in order to find a representative feature set classifying the two groups. The best classification accuracy was achieved using Random Forests and five features of area and slope of lead X.

Table 28: Statistical significance of P-wave features. Bold entries indicate statistical significance both with and without time scaling (normalizing to a 60bpm HR). Asterisks (*) denote no significant differences. Non-bold entries denote differences only with time scaling. μ:mean, σ:standard deviation, *cv*:coefficient of variability, *max*:maximum, *min*:minimum

Features	μ	σ	*cv*	*max*	*min*
P_d	*	1.4853e-05	1.0088e-07	**4.9257e-04**	7.5171e-07
$P_{on}R$	*	**1.3464e-06**	**1.6943e-08**	**3.8277e-04**	9.4417e-08
$P_{of}R$	2.62e-02	**2.0963e-05**	**3.0620e-07**	**0.0051**	**9.5982e-07**
P_a	*	*	*	**2.47e-02**	*
D	**4.7527e-04**	**9.3217e-08**	**4.7527e-04**	**5.6415e-09**	*
A	**6.7020e-06**	*	0.0334	4.4834e-09	*
A_0	**3.4569e-08**	*	1.4853e-05	*	1.4929e-07
ΔA	**9.4114e-09**	*	**1.0947e-10**	**0.0398**	**7.6897e-15**
S_{max}	**4.5521e-05**	**3.6910e-04**	7.6e-03	**1.48e-02**	**2.2829e-05**
$S_{5\%}$	*	**1.68e-02**	*	*	*
$S_{10\%}$	*	**0.62e-02**	*	*	*
$S_{20\%}$	*	**0.13e-02**	*	*	*

Significant differences were observed in P-wave features among the groups in X and Y lead (see Table 28 and Table 29). The statistical analysis shows that P-wave duration in lead X is statistically significant in its maximum value with and without time scaling while in lead Y is only without. In addition, $P_{on}R$ and $P_{of}R$ are statistically significant almost in all measures of X lead whereas the measurements in

Y lead indicate differences before and after time scaling only in their maximum. Moreover, euclidean distance D in lead X presents statistical differences in all measures except minimum but in lead Y is only significant on its coefficient variation and maximum. Area features A, A_o in lead X are significantly different before and after time scaling in their mean as also the A_o in lead Y. The slope features especially S_{max} is statistically significant in both leads X and Y as also $S_{5\%}$ and $S_{20\%}$ in their standard deviation.

Table 29: Statistical significance of P-wave features at lead Y. Bold entries indicate statistical significance both with and without time scaling (normalizing to a 60bpm HR). Asterisks (*) denote no significant differences. Non-bold entries denote differences only with time scaling. μ:mean, σ:standard deviation, *cv*:coefficient of variability, *max*:maximum, *min*:minimum

Features	μ	σ	*cv*	*max*	*min*
P_d	*	*	4.5521e-05	0.0484	3.6910e-04
$P_{on}R$	0.0334	5.9870e-06	1.4173e-07	**0.0042**	2.7046e-05
$P_{of}R$	*	0.0032	4.1155e-04	**0.0092**	2.3255e-04
D	*	*	**4.4540e-06**	**0.0075**	*
A	*	*	*	5.1047e-04	*
A_0	**0.0031**	*	*	*	**0.0012**
S_{max}	**0.0427**	**0.0126**	**0.0447**	**1.48e-02**	**0.0359**
$S_{5\%}$	*	0.0253*	*	*	*
$S_{10\%}$	*	*	*	*	*
$S_{20\%}$	*	**0.0484**	*	0.0354*	*

Several feature selection methods were tested in this work. The OOB method revealed several FVs although a vector of 10 features of area, slope, time-domain features as P_d, $P_{on}R$ and euclidean distance D achieved ACC=93.67% (Table 24). Moreover, MV method highlighted a FV consisted of slope, euclidean distance and mostly area features, presenting an ACC=92.97% (Table 25). Furthermore, features of slope (which were greater in number), area, and D formed a FV based on OCI, yielding an ACC=93.22% (Table 26). In addition, we examined FVs of different lengths as they are summarized in Table 30 and we observed that four features (in total) of area, slope, and D that were chosen especially by OOB method show similar performance as well as the FV of 9 features. However, FVs of length lower than 9, based on MV and OCI methods demonstrated lower classification.

A novel feature of area ΔA which is defined as the difference of A_p from A, was added in the initial FV improving ACC. The best classification accuracy of 95.01% was obtained using features of slope, and area ΔA. Additionally, we demonstrated in Table 31 that adding the next feature or subtracting the least one based on OOB importance did not contribute further to ACC. Interestingly, our classification results using features of lead Y differ from those of lead X. We tested several feature selection methods and various lengths of FVs which exhibited inadequate and poor classification performance below 80%

Table 30: Summary of classification results using OOB, MV, OCI

Feature Sets	ACC	SE	SP
$[\mu A, \mu A_0, cvS_{max}, cvD, stdS_{20\%}$ $stdS_{max}, maxA, minS_{max}, cvP_d]$	**93.70 ± 1.10**	**95.26 ± 2.00**	**91.86±3.82**
$[\mu A_0, stdS_{10\%}, minA_0, maxA,$ $maxS_{max}, \mu A, maxD, cvA, cvA_0]$	91.06 ±1.58	89.90±3.02	92.37 ±3.03
$[\mu A_0, \mu A, stdS_{max}, cvA, stdS_{20\%},$ $stdS_{5\%}, stdS_{10\%}, maxS_{max}, maxA_0]$	92.4 ± 1.16	93.10± 2.52	91.57± 2.94
$[\mu A_0, cvS_{max}, cvD, stdS_{20\%}$ $stdS_{max}, cvP_d]$	**93.07 ± 2.00**	**94.81 ± 4.66**	**91.03± 3.48**
$[maxA, minA_0, \mu A,$ $minS_{max}, maxD, cvA]$	86.47 ±2.69	86.36±3.68	86.47 ±3.44
$[cvA, stdS_{max}, maxA_0,$ $maxS_{max}, stdS_{5\%}, stdS_{10\%}]$	87.86 ± 1.73	87.07± 2.98	88.90± 3.06
$[\mu A_0, cvD, stdS_{20\%}, stdS_{max}]$	**92.34 ±1.49**	**94.47 ± 2.94**	**89.83±3.10**
$[\mu A, minA_0, maxA, cvA]$	87.01 ±2.01	86.52±3.78	87.47 ±3.98
$[stdS_{max}, maxS_{max}, cvA, maxA_0]$	86.19 ± 2.08	85.64± 3.00	86.80± 3.10

Ranked Feature sets of length l=9,6,4, 1st row OOB,2nd row MV, 3rd row OCI

(see Table 32).

The predictive value of maximum P-wave duration, measured in 12-leads has been referred to literature. P-wave duration (P_d) is an electrocardiographic measurement that reflects cardiac conduction through the atria and its prolonged or shortened duration is related to AF recurrence. We estimated the maximum of P_d in a beat-to-beat approach for each subject and statistical differences were presented before and after HR-normalization in lead X, while in lead Y before time scaling in agreement with [58, 59]. We observed that the variability of P_d seems to be more significant as it was selected and participated in FVs of high classification performance (see Table 30). Unfortunately, P_d is likely to be characterized as an unreliable index because it tends to be prolonged in older subjects, and also there is not a clear cut-off value for group discrimination [60].

Our findings confirm that Euclidean distance metric D as a beat-to-beat morphological variability

Table 31: Classification results using ΔA feature testing various lengths FVs based on OOB

Feature Sets	ACC	SE	SP
$[\mu\Delta A, \mu S_{max}, \sigma S_{20\%}, \sigma S_{max}, min\Delta A, minS_{max}]$	94.14 ± 1.04	94.64 ± 1.96	93.56±2.28
$[\mu\Delta A, \sigma S_{20\%}, \sigma S_{max}, min\Delta A, minS_{max}]$	**95.01 ± 0.91**	**95.47 ± 2.03**	**94.43±3.56**
$[\mu\Delta A, \sigma S_{max}, min\Delta A, minS_{max}]$	93.42 ± 1.92	93.71 ± 2.48	93.06±3.96

Table 32: Classification results in lead Y

Feature Sets	ACC	SE	SP	Method
[μA_0, μS_{max}, cvS_{max}, $stdS_{20\%}$,$stdS_{max}$,$stdS_{10\%}$,$minS_{max}$]	77.69 ± 2.26	78.43 ± 3.46	76.77 ± 2.97	min cond.
[cvD,$stdS_{20\%}$,$stdS_{5\%}$ $stdD$, $maxS_{20\%}$, $maxA$, $maxS_{max}$]	76.54 ± 2.6	78.4 ± 2.83	74.53± 2.86	max det
[μS_{max}, cvS_{max}, $stdS_{5\%}$, $stdS_{max}$,$stdD$,$maxS_{20\%}$,$maxS_{max}$]	76.15 ± 2.59	79.76± 2.9	71.8± 4.84	MV
[cvD,$stdS_{10\%}$, $stdD$,$maxS_{20\%}$, $maxA$,$maxS_{max}$,$minA_0$]	**78.49 ±2.16**	**80.79±3.3**	**75.43 ±3.8**	OCI

index has predictive value similarly to [25] and may offer a view of electrophysiological alterations in the atria. In particular, the standard deviation of D was significantly higher in PAF than healthy subjects in lead X than in lead Y that were no significant differences. The coefficient variation of D contributes to the second higher classification accuracy of 93.7% (see Table 30). Additionally, we observed significant differences at their maximum and coefficient of variability values in both leads and D was chosen in many of the tested feature sets for classification tasks.

P-wave area is associated with atrial activity and was investigated in several studies examining stroke risk and AF [61, 62, 63, 26, 64]. P-wave area is a marker for abnormal atrial structure e.g., left atrial enlargement and it has been proposed as a risk indicator for AF [65]. We first explored beat-to-beat variations of P-wave integrals using statistical measures and the mean area features μA at both leads also μA_0 in lead Y demonstrated significant differences. Moreover, they were key features in classification performance, specifically μA_0 of lead X has a strong discrimination ability classifying the groups with an accuracy of 81.2%. Furthermore, we observed that maximum P-wave amplitude in lead X has higher

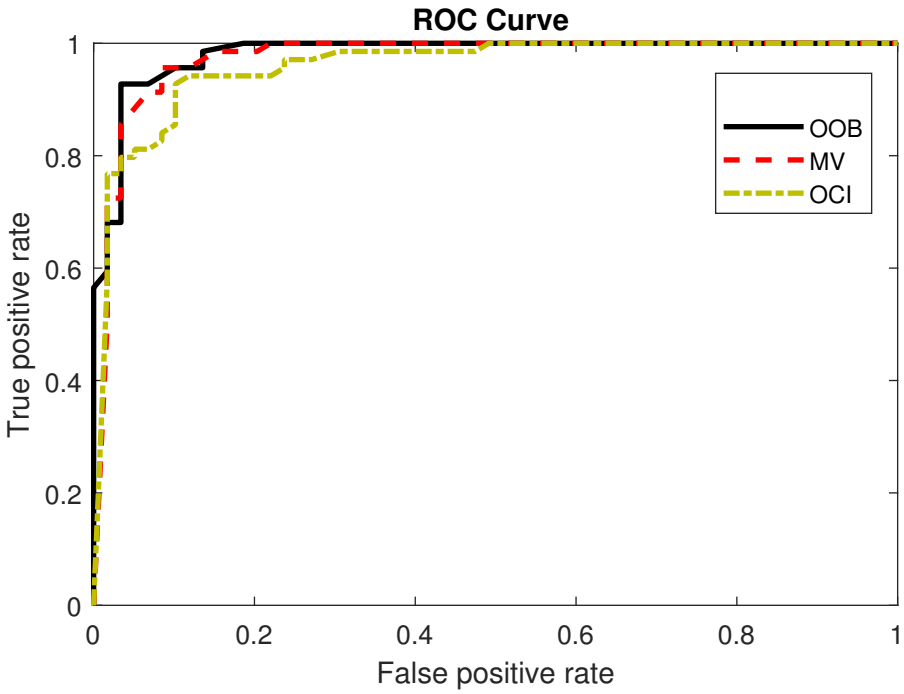

Figure 19: ROC curve based on Table 27 classification results.

voltage values in PAF patients than healthy controls (PAF $156 \pm 194mV$ vs.$91 \pm 70mV$ Healthy).

We introduced for the first time slope features to quantify the P-wave changes during SR. To date slope indices were applied on QRS complex for the detection of myocardial infarction examining its upward and downward slopes [66]. We observed at lead X a steeper S_{max} slope after HR adjustment in mean and minimum of healthy subjects whereas in standard deviation and maximum was lower. Moreover, the standard deviation of S_{max} was involved in all FVs whereas the standard deviation of slope along with area features composed a FV that demonstrated the third higher performance of ACC=93.22% using OCI FS method (see Table 26). It is surprising that S_{max} in lead Y presents significant differences in all statistical measures before and after time scaling as well as $S_{20\%}$ in standard deviation.

Our results are in line with study [27] in which was observed less significant differences in the features extracted from lead Y. Studies based on VCG have shown that the right and left atrial components are best viewed in the horizontal plane (X and Z axis). As far as we know, P-wave intervals on the vectorcardiographic records were divided into the first half as the right atrial depolarization and the second half of the left atrial depolarization [67]. However, in the horizontal plane, the early right and the left atrial component are divided without overlapping whereas in the Y lead the P-wave is fused [27, 67].

A receiver operating characteristic (ROC) curve is a graph of sensitivity against 1 – specificity de-

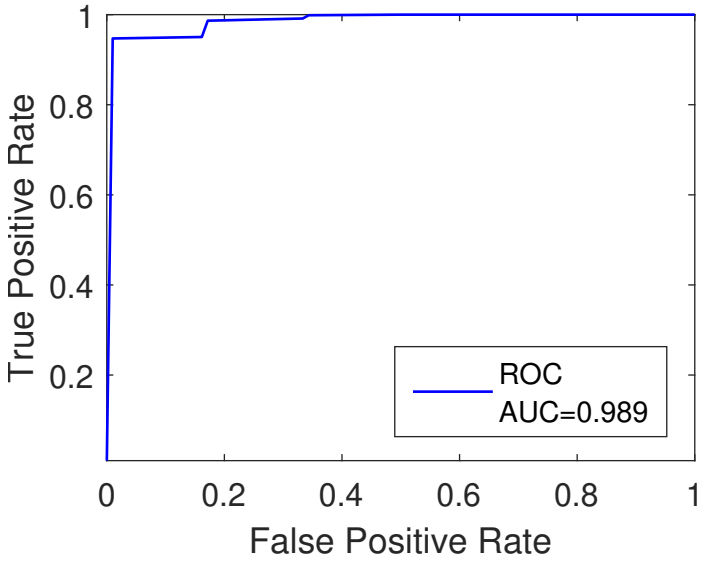

Figure 20: Mean ROC curve over 10 repetitions per fold, 10-folds of best FV.

picting the diagnostic ability of a binary classifier system as its discrimination threshold is varied. Each prediction result of the confusion matrix is represented by one point in the ROC space. A perfect test has sensitivity, specificity, and area under the ROC curve (AUC) both equal to 1 in which AUC is calculated as a sum of the areas of trapeziums [68]. We calculated the ROC curve (see Figure 20) of FV with the best classification results presenting AUC=0.989, ACC=95.01%. Additionally, in Figure 19 we can observe a graphical comparison of the best FV versus FVs of same length that were proposed by MV and OCI methods, demonstrating lower AUC as well as ACC.

The ventricular conduction system and also the intra-atrial conduction are affected by the autonomic nervous system [45]. It is known that a strong correlation between QT interval and HR exists. In study [69] P-wave area, P_d and $P_{on}R$ exhibited circadian variation as autonomic nervous influence. Moreover, the PQ interval which is defined as the time between P-onset and QRS complex onset is heart rate (HR) dependant and is linearly associated [45]. In an attempt to control HR influence, many formulas as linear power, logarithmic and cubic function can minimize the influence implementing HR adjustment. In a similar vein, we applied time scaling on a beat-to-beat basis in order to normalize our metrics to a nominal 60 bpm HR and was simpler than the methods used by others [47].

The PAF is characterized by rapid and self-terminating episodes alternating with SR. Therefore, PAF prediction during the SR is challenging and almost one-third of patients are not aware that are affected due to the condition's asymptomatic nature. Nowadays, AF can be detected by wearables devices using PPG which are abundant and FDA approved. However, their use on daily basis as a healthcare

diagnostic tool has raised some concerns. Their accuracy can be affected by motion artifact, ectopic beats, peripheral vascular disease, poor skin contact, and limited battery life. Besides, a proportion of false-positive results may occur in lower-risk individuals leading to anxiety, healthcare costs, and inappropriate treatment. Moreover, another limitation arises in the affordability of devices capable of AF detection [14, 13].

In contrast to wearable PPG-based devices, we propose a clinical examination tool for AF identification in short-term ECG recordings while the patient is under SR and there is no visible sign of AF on ECG. The early detection of a possible PAF incidence is valuable especially when the individual is asymptomatic, identifying patients at risk. Our non-invasive method can be used in clinical practice avoiding long-term electrocardiographic evaluations that increase healthcare costs. In a non-time-consuming approach, patients management can be facilitated by enhancing their awareness and initiating treatment, thus improving their quality of life. Early interventions such as pharmacological or restoration of SR can be used to avert PAF progression to an AF persistent type.

5.2 Comparison with state of the art

Table 33: Performance of the algorithms for PAF prediction during SR

Dataset	ACC	SE	SP	AUC	Features	PAF	Healthy
Martínez *et al.* [26]	86.33%	-	-	-	V1 lead, 5min	46	53
Conte *et al.* [25]	88%	92%	83%	-	lead II, 5min	76	40
Vassilikos *et al.* [28]	-	-	-	85%	X and Z lead, 10 min	50	50
Filos *et al.* [27]	93.75%	100%	87.5%	-	X, Y, Z lead, 10 min	29	25
Attia *et al.* [23]	83.3%	82.3%	83.4%	0.90	leads I,II, V1-V6, 10 sec	180922	N/D
Chen *et al.* [24]	79.9%	-	-	0.90	V5 lead, 10 sec	59	38
Proposed method	95.01%	95.47%	94.43%	0.98	lead X, 10 min	69	59

Our classification results can be compared directly, and favorably, with several previous studies that have attempted to discriminate subjects with PAF from healthy ones, all during the SR (see Table 33). In [26] P-wave indices similar to our own (arc length and the area A) were used to achieve an average

classification accuracy of 86.33% in which 94.48% among 53 healthy vs. PAF as well as 86.96% far from PAF (1h away from the onset) vs. close to PAF (1h immediately before the onset). In their approach was used a decision tree and 1hr of ECG recordings fs=1000 Hz, (V1 lead) which were taken 2hrs prior to the PAF onset of 46 patients. Another study, using linear discriminant analysis (LDA) reported an accuracy of ACC=88% using P-wave duration and beat-to-beat Euclidean distance as the main features [25]. They used 5 min ECG recordings of 76 PAF and 40 healthy individuals, fs=1000 Hz (lead II), and PAF patients who had at least 2 previous PAF episodes. In [28] the occurrence of PAF was predicted using P-wave duration and mean P-wave energy with AUC=85% (X and Z lead) by means of logistic regression and ECGs of 10 min, fs=1000 Hz that were recorded 7 days after SR restoration in 50 PAF patients and 50 healthy controls selecting only thirty consecutive P-waves for analysis.

More recently, [27] achieved an accuracy of 93.75% by analyzing beat-to-beat P-wave morphology and time-frequency domain features in ECGs of X, Y, Z lead of 3-5min, fs=1000 Hz in 29 PAF and 25 healthy, using wavelets and support vector machines (SVMs). Among the works mentioned here, the classification accuracy of [27] was closest to ours and involved higher computational complexity. The authors of [23] reported an accuracy of 83.3% using ECGs that are collected 31 days before the first recorded PAF occurrence in a large cohort of 180922 positives for AF (at least 1 recorded AF episode) and negative for AF patients with 649931 normal sinus rhythm ECGs using convolutional neural networks and eight independent leads (leads I, II, and V1–6) from 12-lead ECG, fs=500Hz of 10sec duration as inputs. Along similar lines, with the addition of demographic data, [22] achieved ACC=79.9% using 10 sec of 12-lead ECG (V5 lead) fs=400 Hz of 59 PAF patients and 38 healthy. One of the drawbacks to adopting deep learning methods is the large amounts of available data and processing power required, as well as potential challenges in terms of explainability [70]. In our case, we were able to classify subjects with an accuracy that was higher than the aforementioned approaches and a relatively lower complexity model, using a novel feature set.

6 Conclusions

In this study, we have analyzed beat-to-beat P-waves of ECG signals during the SR of PAF and healthy subjects. We extracted time-domain, slope, and area features in each cardiac cycle of lead X and Y, observing significant differences between the groups. We evaluated the features before as well as after applying a time scale factor diminishing the HR influence on our P-wave based features. We formed after a feature selection process feature vectors testing several feature combinations. We succeeded a state of the art classification accuracy using Random Forests and a feature vector consisted of five novel features of slope and area, discriminating the groups with 95% accuracy.

6.1 Implications of study

The present findings have important implications for the early PAF detection averting its progression and invasive procedures. One promising application of our technique would be as a digital tool in clinical practice along with ECG examination. Therefore, the patients will be informed by the electrophysiologist to be aware of a possible PAF occurrence even if they are not experienced any symptoms. Additionally, our approach is beneficial in solving the difficulty of PAF identification eliminating the long-term ECG recordings and healthcare costs in order to detect an AF incidence. The management of patients with PAF history can be done by discerning low and high-risk groups, increasing the outpatient visits in a short follow-up period, and starting the treatment without delay.

6.2 Limitations and Future work

Our study considered only signals from the X and Y lead in the ECG recordings. Incorporating signals from Z lead could further improve classification accuracy due to it offers a better view of atrial components. We analyzed P-waves that are positive and discarded negative or biphasic. The analysis and extraction of P-waves that are changing morphology during an ECG recording may offer a thorough examination of atrial activity. Previous studies have indicated the role of P-wave morphology in PAF detection examining X, Y, Z leads. Also, an electrophysiology interpretation of the novel area feature ΔA may shed light upon AF pathophysiology, explaining why significant differences were observed between healthy and PAF groups. Statistical comparison of features before and after the time scale application would be needed to investigate the HR influence on atrial-based extracted features. Furthermore, we aware that the comparison of our study with other studies may lead to discrepancies because of the different size of data sets and the dissimilar duration of ECG recordings.

Our results are encouraging and should be validated by larger sample size. Further work needs

to be performed to establish whether correlations exist among the extracted features and evaluate the factors (age, co-morbidities, lifestyle) that can affect the PAF incidence. Also, a prospective study is warranted to investigate the predictive and clinical utility of our approach. Several months of follow-up for the PAF group should be considered to observe if the identified PAF patients will actually develop AF. Future research is also needed to determine how accurate is the proposed method based on the PAF time occurrence. Is it affected if the PAF incidence is close to the time frame that has been chosen for evaluation?

Bibliography

[1] S. Prabhu and A. Sohaib, "The basic language of cardiac electrophysiology—An introduction to intracardiac electrograms and electrophysiology studies," in *Decoding Cardiac Electrophysiology*, pp. 3–19, Springer, 2020.

[2] A. Davies and A. Scott, "ECG interpretation," in *Starting to Read ECGs*, pp. 17–43, Springer, 2015.

[3] R. Klabunde, *Cardiovascular physiology concepts*. Lippincott Williams & Wilkins, 2011.

[4] A. L. Goldberger, Z. D. Goldberger, and A. Shvilkin, *Clinical electrocardiography: a simplified approach e-book*. Elsevier Health Sciences, 2017.

[5] G. Hindricks, T. Potpara, N. Dagres, E. Arbelo, J. J. Bax, C. Blomström-Lundqvist, G. Boriani, M. Castella, G.-A. Dan, P. E. Dilaveris, L. Fauchier, G. Filippatos, J. M. Kalman, M. La Meir, D. A. Lane, J.-P. Lebeau, M. Lettino, G. Y. H. Lip, F. J. Pinto, G. N. Thomas, M. Valgimigli, I. C. Van Gelder, B. P. Van Putte, C. L. Watkins, and E. S. D. Group, "2020 ESC Guidelines for the diagnosis and management of atrial fibrillation developed in collaboration with the European Association of Cardio-Thoracic Surgery (EACTS): The Task Force for the diagnosis and management of atrial fibrillation of the European Society of Cardiology (ESC) Developed with the special contribution of the European Heart Rhythm Association (EHRA) of the ESC," *European Heart Journal*, 08 2020.

[6] P. Singh, I. Srivastava, A. Singhal, and A. Gupta, "Baseline wander and power-line interference removal from ECG signals using fourier decomposition method," in *Machine Intelligence and Signal Analysis*, pp. 25–36, Springer, 2019.

[7] S. K. Paul, C. K. Choubey, and G. Tiwari, "Low power analog comb filter for biomedical applications," *Analog Integrated Circuits and Signal Processing*, vol. 97, no. 2, pp. 371–386, 2018.

[8] A. B. De Luna, V. N. Batchvarov, and M. Malik, "The morphology of the electrocardiogram," *The ESC Textbook of Cardiovascular Medicine Blackwell Publishing*, vol. 35, 2006.

[9] F. Holmqvist, P. G. Platonov, R. Havmöller, and J. Carlson, "Signal-averaged P-wave analysis for delineation of interatrial conduction–further validation of the method," *BMC cardiovascular disorders*, vol. 7, no. 1, p. 29, 2007.

[10] A. Herreros, E. Baeyens, R. Johansson, J. Carlson, J. R. Perán, and B. Olsson, "Analysis of changes in the beat-to-beat P-wave morphology using clustering techniques," *Biomedical Signal Processing and Control*, vol. 4, no. 4, pp. 309–316, 2009.

[11] A. Rizwan, A. Zoha, I. Mabrouk, H. Sabbour, A. Al-Sumaiti, A. Alomaniy, M. Imran, and Q. Abbasi, "A review on the state of the art in atrial fibrillation detection enabled by machine learning," *IEEE Reviews in Biomedical Engineering*, 2020.

[12] P. E. Dilaveris and H. L. Kennedy, "Silent atrial fibrillation: epidemiology, diagnosis, and clinical impact," *Clinical Cardiology*, vol. 40, no. 6, pp. 413–418, 2017.

[13] K. Rajakariar, A. N. Koshy, J. K. Sajeev, S. Nair, L. Roberts, and A. W. Teh, "Accuracy of a smartwatch based single-lead electrocardiogram device in detection of atrial fibrillation," *Heart*, vol. 106, no. 9, pp. 665–670, 2020.

[14] E. Y. Ding, G. M. Marcus, and D. D. McManus, "Emerging technologies for identifying atrial fibrillation," *Circulation Research*, vol. 127, no. 1, pp. 128–142, 2020.

[15] M. Dörr, V. Nohturfft, N. Brasier, E. Bosshard, A. Djurdjevic, S. Gross, C. J. Raichle, M. Rhinisperger, R. Stöckli, and J. Eckstein, "The WATCH AF trial: Smartwatches for detection of atrial fibrillation," *JACC: Clinical Electrophysiology*, vol. 5, no. 2, pp. 199–208, 2019.

[16] C. R. Lopez Perales, H. G. Van Spall, S. Maeda, A. Jimenez, D. G. Laţcu, A. Milman, F. Kirakoya-Samadoulougou, M. A. Mamas, D. Muser, and R. Casado Arroyo, "Mobile health applications for the detection of atrial fibrillation: a systematic review," *EP Europace*, 2020.

[17] A. Jalali and M. Lee, "Atrial fibrillation prediction with residual network using sensitivity and orthogonality constraints," *IEEE Journal of Biomedical and Health Informatics*, vol. 24, no. 2, pp. 407–413, 2019.

[18] H. Dang, M. Sun, G. Zhang, X. Qi, X. Zhou, and Q. Chang, "A novel deep arrhythmia-diagnosis network for atrial fibrillation classification using electrocardiogram signals," *IEEE Access*, vol. 7, pp. 75577–75590, 2019.

[19] X. Fan, Q. Yao, Y. Cai, F. Miao, F. Sun, and Y. Li, "Multiscaled fusion of deep convolutional neural networks for screening atrial fibrillation from single lead short ECG recordings," *IEEE journal of biomedical and health informatics*, vol. 22, no. 6, pp. 1744–1753, 2018.

[20] D. Dobreanu, J. H. Svendsen, T. Lewalter, A. Hernández-Madrid, G. Y. Lip, C. Blomström-Lundqvist, and E. H. R. A. conducted by the Scientific Initiatives Committee, "Current practice for diagnosis and management of silent atrial fibrillation: results of the european heart rhythm association survey," *Europace*, vol. 15, no. 8, pp. 1223–1225, 2013.

[21] R. L. Page, T. W. Tilsch, S. J. Connolly, D. J. Schnell, S. R. Marcello, W. E. Wilkinson, and E. L. Pritchett, "Asymptomatic or "silent" atrial fibrillation: frequency in untreated patients and patients receiving azimilide," *Circulation*, vol. 107, no. 8, pp. 1141–1145, 2003.

[22] Y.-H. Chen, A. H. Twing, D. Badawi, J. Danavi, M. McCauley, and A. E. Cetin, "Atrial fibrillation risk prediction from electrocardiogram and related health data with deep neural network," in *ICASSP 2020-2020 IEEE International Conference on Acoustics, Speech and Signal Processing (ICASSP)*, pp. 1269–1273, IEEE, 2020.

[23] Z. I. Attia, P. A. Noseworthy, F. Lopez-Jimenez, S. J. Asirvatham, A. J. Deshmukh, B. J. Gersh, R. E. Carter, X. Yao, A. A. Rabinstein, B. J. Erickson, *et al.*, "An artificial intelligence-enabled ECG algorithm for the identification of patients with atrial fibrillation during sinus rhythm: a retrospective analysis of outcome prediction," *The Lancet*, vol. 394, no. 10201, pp. 861–867, 2019.

[24] L. Y. Y. Chen and E. Z. Soliman, "P wave indices—advancing our understanding of atrial fibrillation-related cardiovascular outcomes," *Frontiers in cardiovascular medicine*, vol. 6, p. 53, 2019.

[25] G. Conte, A. Luca, S. Yazdani, M. L. Caputo, F. Regoli, T. Moccetti, L. Kappenberger, J.-M. Vesin, and A. Auricchio, "Usefulness of P-wave duration and morphologic variability to identify patients prone to paroxysmal atrial fibrillation," *The American journal of cardiology*, vol. 119, no. 2, pp. 275–279, 2017.

[26] A. Martínez, R. Alcaraz, and J. J. Rieta, "Morphological variability of the P-wave for premature envision of paroxysmal atrial fibrillation events," *Physiological measurement*, vol. 35, no. 1, p. 1, 2013.

[27] D. Filos, I. Chouvarda, D. Tachmatzidis, V. Vassilikos, and N. Maglaveras, "Beat-to-beat P-wave morphology as a predictor of paroxysmal atrial fibrillation," *Computer methods and programs in biomedicine*, vol. 151, pp. 111–121, 2017.

[28] V. Vassilikos, G. Dakos, Y. S. Chatzizisis, I. Chouvarda, C. Karvounis, C. Maynard, N. Maglaveras, S. Paraskevaidis, G. Stavropoulos, C. I. Styliadis, *et al.*, "Novel non-invasive P-wave analysis for the prediction of paroxysmal atrial fibrillation recurrences in patients without structural heart disease: a prospective pilot study," *International journal of cardiology*, vol. 153, no. 2, pp. 165–172, 2011.

[29] M. Thaler, *The only EKG book you'll ever need*. Lippincott Williams & Wilkins, 2017.

[30] L. Staerk, J. A. Sherer, D. Ko, E. J. Benjamin, and R. H. Helm, "Atrial fibrillation: epidemiology, pathophysiology, and clinical outcomes," *Circulation research*, vol. 120, no. 9, pp. 1501–1517, 2017.

[31] D. H. Lau, D. Linz, U. Schotten, R. Mahajan, P. Sanders, and J. M. Kalman, "Pathophysiology of paroxysmal and persistent atrial fibrillation: rotors, foci and fibrosis," *Heart, Lung and Circulation*, vol. 26, no. 9, pp. 887–893, 2017.

[32] T. Potpara, N. Dagres, E. Arbelo, G. Boriani, M. Castella, and G.-A. Dan, "2020 ESC Guidelines for the diagnosis and management of atrial fibrillation developed in collaboration with the european association of cardio-thoracic surgery (EACTS): Supplementary data,"

[33] N. M. de Groot and M. A. Allessie, "Pathophysiology of atrial fibrillation: Focal patterns of activation," *Pacing and Clinical Electrophysiology*, vol. 42, no. 10, pp. 1312–1319, 2019.

[34] L. Neubeck, J. Orchard, N. Lowres, and S. B. Freedman, "To screen or not to screen? Examining the arguments against screening for atrial fibrillation," *Heart, Lung and Circulation*, vol. 26, no. 9, pp. 880–886, 2017.

[35] S. R. Steinhubl, J. Waalen, A. M. Edwards, L. M. Ariniello, R. R. Mehta, G. S. Ebner, C. Carter, K. Baca-Motes, E. Felicione, T. Sarich, *et al.*, "Effect of a home-based wearable continuous ECG monitoring patch on detection of undiagnosed atrial fibrillation: the mstops randomized clinical trial," *Jama*, vol. 320, no. 2, pp. 146–155, 2018.

[36] S. Mittal, C. Movsowitz, and J. S. Steinberg, "Ambulatory external electrocardiographic monitoring: focus on atrial fibrillation," *Journal of the American College of Cardiology*, vol. 58, no. 17, pp. 1741–1749, 2011.

[37] A. R. P. Riera, A. H. Uchida, C. Ferreira Filho, A. Meneghini, C. Ferreira, E. Schapacknik, S. Dubner, and P. Moffa, "Significance of vectorcardiogram in the cardiological diagnosis of the 21st century," *Clinical cardiology*, vol. 30, no. 7, p. 319, 2007.

[38] R. Jaros, R. Martinek, and L. Danys, "Comparison of different electrocardiography with vectorcardiography transformations," *Sensors*, vol. 19, no. 14, p. 3072, 2019.

[39] "Lead system," *Acta Medica Scandinavica*, vol. 178, no. S440, pp. 9–13, 1965.

[40] L. Sörnmo and P. Laguna, "Electrocardiogram (ECG) signal processing," *Wiley encyclopedia of biomedical engineering*, 2006.

[41] P. G. Malghan and M. K. Hota, "A review on ECG filtering techniques for rhythm analysis," *Research on Biomedical Engineering*, pp. 1–16, 2020.

[42] K. Venkatachalam, J. E. Herbrandson, and S. J. Asirvatham, "Signals and signal processing for the electrophysiologist: part i: electrogram acquisition," *Circulation: Arrhythmia and Electrophysiology*, vol. 4, no. 6, pp. 965–973, 2011.

[43] P. G. Platonov, "P-wave morphology: underlying mechanisms and clinical implications," *Annals of Noninvasive Electrocardiology*, vol. 17, no. 3, pp. 161–169, 2012.

[44] J. Pan and W. J. Tompkins, "A real-time QRS detection algorithm," *IEEE Trans. Biomed. Eng*, vol. 32, no. 3, pp. 230–236, 1985.

[45] O. Toman, K. Hnatkova, P. Smetana, K. M. Huster, M. Šišáková, P. Barthel, T. Novotnỳ, G. Schmidt, and M. Malik, "Physiologic heart rate dependency of the PQ interval and its sex differences," *Scientific Reports*, vol. 10, no. 1, pp. 1–17, 2020.

[46] E. Z. Soliman and P. M. Rautaharju, "Heart rate adjustment of PR interval in middle-aged and older adults," *Journal of electrocardiology*, vol. 45, no. 1, pp. 66–69, 2012.

[47] S. W. Rabkin, E. Szefer, and D. J. Thompson, "A new QT interval correction formulae to adjust for increases in heart rate," *JACC: Clinical Electrophysiology*, vol. 3, no. 7, pp. 756–766, 2017.

[48] S. C. Chapra, R. P. Canale, *et al.*, *Numerical methods for engineers*. Boston: McGraw-Hill Higher Education,, 2010.

[49] I. Guyon and A. Elisseeff, "An introduction to variable and feature selection," *Journal of machine learning research*, vol. 3, no. Mar, pp. 1157–1182, 2003.

[50] Y. Saeys, I. Inza, and P. Larrañaga, "A review of feature selection techniques in bioinformatics," *bioinformatics*, vol. 23, no. 19, pp. 2507–2517, 2007.

[51] S. A. Goreinov, I. V. Oseledets, D. V. Savostyanov, E. E. Tyrtyshnikov, and N. L. Zamarashkin, "How to find a good submatrix," in *Matrix Methods: Theory, Algorithms And Applications: Dedicated to the Memory of Gene Golub*, pp. 247–256, World Scientific, 2010.

[52] H. F. Inman and E. L. Bradley Jr, "The overlapping coefficient as a measure of agreement between probability distributions and point estimation of the overlap of two normal densities," *Communications in Statistics-Theory and Methods*, vol. 18, no. 10, pp. 3851–3874, 1989.

[53] P. C. Austin and J. E. Hux, "A brief note on overlapping confidence intervals," *Journal of vascular surgery*, vol. 36, no. 1, pp. 194–195, 2002.

[54] B. Liu, *Web data mining: exploring hyperlinks, contents, and usage data*. Springer Science & Business Media, 2007.

[55] L. Breiman, "Random forests," *Machine learning*, vol. 45, no. 1, pp. 5–32, 2001.

[56] R. Kohavi *et al.*, "A study of cross-validation and bootstrap for accuracy estimation and model selection," in *Ijcai*, vol. 14, pp. 1137–1145, Montreal, Canada, 1995.

[57] P. Baldi, S. Brunak, Y. Chauvin, C. A. Andersen, and H. Nielsen, "Assessing the accuracy of prediction algorithms for classification: an overview," *Bioinformatics*, vol. 16, no. 5, pp. 412–424, 2000.

[58] P. E. Dilaveris, E. J. Gialafos, S. K. Sideris, A. M. Theopistou, G. K. Andrikopoulos, M. Kyriakidis, J. E. Gialafos, and P. K. Toutouzas, "Simple electrocardiographic markers for the prediction of paroxysmal idiopathic atrial fibrillation," *American heart journal*, vol. 135, no. 5, pp. 733–738, 1998.

[59] E. Yıldırım, N. Günay, E. Bayam, M. Keskin, B. Ozturkeri, and M. Selcuk, "Relationship between paroxysmal atrial fibrillation and a novel electrocardiographic parameter P wave peak time," *Journal of electrocardiology*, vol. 57, pp. 81–86, 2019.

[60] G. Q. Villani, M. Piepoli, A. Rosi, and A. Capucci, "P-wave dispersion index: a marker of patients with paroxysmal atrial fibrillation," *International journal of cardiology*, vol. 55, no. 2, pp. 169–175, 1996.

[61] H. Kamel, E. Z. Soliman, S. R. Heckbert, R. A. Kronmal, W. Longstreth Jr, S. Nazarian, and P. M. Okin, "P-wave morphology and the risk of incident ischemic stroke in the Multi-Ethnic Study of Atherosclerosis," *Stroke*, vol. 45, no. 9, pp. 2786–2788, 2014.

[62] J. He, G. Tse, P. Korantzopoulos, K. P. Letsas, S. Ali-Hasan-Al-Saegh, H. Kamel, G. Li, G. Y. Lip, and T. Liu, "P-wave indices and risk of ischemic stroke: a systematic review and meta-analysis," *Stroke*, vol. 48, no. 8, pp. 2066–2072, 2017.

[63] K. Van Beeumen, R. Houben, R. Tavernier, S. Ketels, and M. Duytschaever, "Changes in P-wave area and P-wave duration after circumferential pulmonary vein isolation," *Europace*, vol. 12, no. 6, pp. 798–804, 2010.

[64] J. W. Weinsaft, J. D. Kochav, J. Kim, S. Gurevich, S. C. Volo, A. Afroz, M. Petashnick, A. Kim, R. B. Devereux, and P. M. Okin, "P wave area for quantitative electrocardiographic assessment of left atrial remodeling," *PloS one*, vol. 9, no. 6, 2014.

[65] D. M. German, M. M. Kabir, T. A. Dewland, C. A. Henrikson, and L. G. Tereshchenko, "Atrial fibrillation predictors: importance of the electrocardiogram," *Annals of Noninvasive Electrocardiology*, vol. 21, no. 1, pp. 20–29, 2016.

[66] E. Pueyo, L. Sornmo, and P. Laguna, "QRS slopes for detection and characterization of myocardial ischemia," *IEEE transactions on Biomedical Engineering*, vol. 55, no. 2, pp. 468–477, 2008.

[67] L. J. Haywood and R. H. Selvester, "Analysis of right and left atrial vectorcardiograms: Timed records of 100 normal persons," *Circulation*, vol. 33, no. 4, pp. 577–587, 1966.

[68] V. Bewick, L. Cheek, and J. Ball, "Statistics review 13: receiver operating characteristic curves," *Critical care*, vol. 8, no. 6, pp. 1–5, 2004.

[69] P. E. Dilaveris, P. Färbom, V. Batchvarov, A. Ghuran, and M. Malik, "Circadian behavior of P-wave duration, P-wave area, and PR interval in healthy subjects," *Annals of noninvasive electrocardiology*, vol. 6, no. 2, pp. 92–97, 2001.

[70] A. K. Feeny, M. K. Chung, A. Madabhushi, Z. I. Attia, M. Cikes, M. Firouznia, P. A. Friedman, M. M. Kalscheur, S. Kapa, S. M. Narayan, P. A. Noseworthy, R. S. Passman, M. V. Perez, N. S. Peters, J. P. Piccini, K. G. Tarakji, S. A. Thomas, N. A. Trayanova, M. P. Turakhia, and P. J. Wang, "Artificial intelligence and machine learning in arrhythmias and cardiac electrophysiology," *Circulation: Arrhythmia and Electrophysiology*, vol. 13, no. 8, p. e007952, 2020.